Artūrs Bogdanovs

RESEARCH AND DEVELOPMENT OF AUXILIARY CONVERTERS FOR APPLICATION IN ELECTRIC VEHICLES

Summary of the Doctoral Thesis
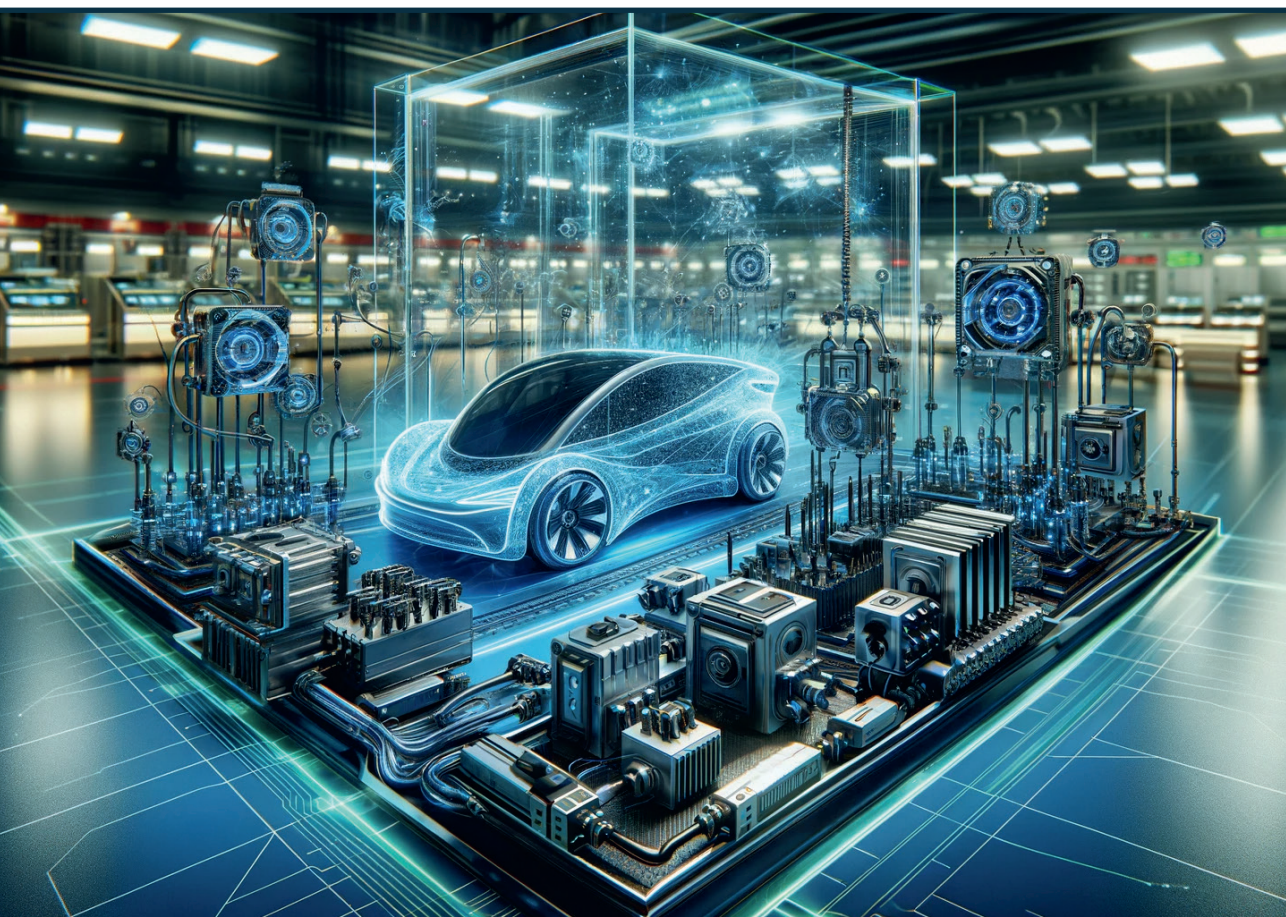
RIGA TECHNICAL UNIVERSITY

Faculty of Electrical and Environmental Engineering
Institute of Industrial Electronics and Electrical Engineering

Artūrs Bogdanovs

Doctoral Student of the Study Programme "Computerised Control of Electrical Technologies"

RESEARCH AND DEVELOPMENT OF AUXILIARY CONVERTERS FOR APPLICATION IN ELECTRIC VEHICLES

Summary of the Doctoral Thesis

Scientific supervisor
Professor Dr. sc. ing.
OSKARS KRIEVS

Scientific advisor
Professor Dr.
JOHANNES PFORR

RTU Press
Riga 2023

NATIONAL DEVELOPMENT PLAN 2020

EUROPEAN UNION
European Social Fund

INVESTING IN YOUR FUTURE

1862

RIGA TECHNICAL UNIVERSITY

Cover picture generated by openAI DALL-E/ChatGPT 4.0.

DOCTORAL THESIS PROPOSED TO RIGA TECHNICAL UNIVERSITY FOR THE PROMOTION TO THE SCIENTIFIC DEGREE OF DOCTOR OF SCIENCE

To be granted the scientific degree of Doctor of Science (Ph. D.), the present Doctoral Thesis has been submitted for defence at the open meeting of RTU Promotion Council on 29 December 2023 13.30 at the Faculty of Electrical and Environmental Engineering of Riga Technical University, Azenes Street 12/1, Room 212.

OFFICIAL REVIEWERS

Assoc. Professor Dr. sc. ing. Jānis Zaķis
Riga Technical University

Senior Researcher Ph. D. Dmitri Vinnikov
Tallinn University of Technology, Estonia

Professor Ph. D. Sonata Tolvaišiene
Vilnius Gediminas technical university, Lithuania

DECLARATION OF ACADEMIC INTEGRITY

I hereby declare that the Doctoral Thesis submitted for review to Riga Technical University for promotion to the scientific degree of Doctor of Science (Ph. D.) is my own. I confirm that this Doctoral Thesis has not been submitted to any other university for the promotion to a scientific degree.

Artūrs Bogdanovs ……………………………. (signature)
Date: ………………………

The Doctoral Thesis has been written in English. It consists of an Introduction, 4 chapters, Conclusions, 66 figures, and 6 tables; the total number of pages is 85. The Bibliography contains 75 titles.

CONTENTS

GENERAL OVERVIEW OF THE THESIS

Motivation and background

The transport sector makes about a quarter of total greenhouse gas emissions in Europe and is, therefore, the main contributor to climate change now. To significantly reduce the environmental footprint, the European Commission has stated a goal to reduce the greenhouse gas emissions in the transport sector by 90 % before 2050. To fulfil this goal, the most effective solution nowadays is the transport sector's transition towards electrified drivetrain technology. The number of electric vehicles has shown a gradual increase within the last decade, and this number is expected to show rapid growth in the future. This raises a lot of concerns regarding vehicle energy consumption and efficiency.

The vehicle energy consumption consists of the energy drawn by the main propulsion (drive) system and auxiliary power required for the rest of the systems located in a vehicle, e.g. lighting, signalling, control, pneumatic and hydraulic systems for steering and braking systems, heating, ventilation and air conditioning (HVAC). In the case of electric vehicles, all the auxiliary systems must be supplied from the vehicle's electrical energy net, and hence, the demand for auxiliary converter power in transportation applications continues to increase. In addition, more safety and comfort systems are being introduced that demand additional auxiliary power and increasing the dimensions and weight of auxiliary converter systems.

Some vehicle auxiliary components, like power steering and braking system, are safety critical, i.e. there are catastrophic consequences in case of failure. Therefore, the fault-tolerance and reliability of auxiliary converter systems becomes crucial aspect and there is a demand for reliable solutions for auxiliary converters. As the component redundancy and the growing power consumption leads to increasing volume and weight, it results in increased overall vehicle energy consumption. Hence, there is a need for cheap, reliable, energy-efficient and environmentally friendly solutions in electric vehicle auxiliary converter design. However, most of the scientific contributions and research results are mainly focused on the advancements in the vehicle main drive systems, while the auxiliary converter systems are often neglected and are not at the top of current research interests, despite the growing industry demands and electric vehicle market potential for growth.

Hypotheses and theses for defence

1. The converter's voltage and current waveforms contain sufficient information about converter status that, combined with intelligent sensing, can be utilized by the control system to ensure improved fault tolerance and more reliable power supply, thus increasing safety in critical auxiliary systems of electric vehicles.
2. Intelligent sensing and converter control systems with integrated status monitoring ensure operation with the highest possible efficiency and optimized performance, even in an active failure mode, by ensuring fast transition to the fault-tolerant operation mode and improving efficiency by up to 2 %.

3. Auxiliary drive design with permanently excited synchronous machine and multi-level inverter utilizing modern wide bandgap semiconductor devices ensures energy savings by 10 %, more reliable, faster operation and is an economically effective solution in scope of the whole converter's life cycle in electric vehicle operation.

Research aim and objectives

The Thesis aims to research and develop an energetically and economically effective technology for auxiliary converter systems in electric vehicles in accordance with the actual industry needs, as well as to create a scientific contribution and disseminate the acquired knowledge by introducing new concepts in the proposed converter design.

The main objectives of the Thesis are:
1. To investigate and develop novel current sensing and measurement techniques in auxiliary converters.
2. To investigate and develop the control methods and to analyse the control performance under unpredictable auxiliary converter load conditions.
3. To develop a solution for fault detection and to investigate fault-tolerant operation capabilities.
4. To analyse the wide bandgap semiconductor device application in auxiliary converters, including the cost vs benefit analysis.
5. To investigate and propose the solution for reliable and energy-saving auxiliary drive operation.

Research object and scope

The main research object of the Thesis is the auxiliary converter system, consisting of non-isolated DC/DC converters and DC/AC inverters for auxiliary drives. The main scope of application is mainly focused on different types of grid-connected electric vehicles and transportation, i.e., trolleybuses, trams, and electric motorized units in light and heavy railways, as well as battery electric vehicles. The proposed concepts and technological improvements may be applied in any type of vehicle auxiliary converter systems in whole or in part. However, the preliminary technology adaptation for the specific vehicle type is always required. The proposed indirect current sensing solution, fault detection and identification technique and fault-tolerant operation algorithms can be used in any application where the DC/DC or DC/AC multiphase or multilevel power converters are utilized.

Research tools and methods

To fulfil the aim of the Thesis, the incremental research design method is being used. The research stages include the determination of the appropriate auxiliary converter topologies, adjusting the converter mathematical model parameters, developing simulation models, evaluating the results of simulations, developing auxiliary converter prototypes and performing

experimental verification in a laboratory environment. The prototypes of a 5-phase bi-directional DC/DC converter with coupled inductors and a 3-phase 3-level DC/AC inverter have been built for the proposed concepts and technological improvements validation in a laboratory environment. Hence, the research results correspond to the Technology Readiness Level 4 (TRL4).

Scientific novelty

1. The novel Indirect Current Measurement (ICM) technique, including the voltage and current sensing circuit part and the phase current reconstruction signal processing part, has been developed and integrated into the DC/DC converter and DC-AC inverter.
2. A fuzzy logic current balancing and output voltage regulation controller with optimized steady-state and dynamic performance has been developed based on the ICM and applied for the DC/DC converter control.
3. The common fault detection and identification method with fast response based on the extended signal processing of ICM has been developed and integrated into the DC/DC converter self-diagnosis system.
4. A fault-tolerant operation algorithm for the multiphase converter with strongly coupled inductors and small reaction time has been developed for reliable power supply to the safety-critical systems.
5. A comparative analysis of the modern wide bandgap SiC and GaN semiconductor application in high-voltage auxiliary converters is performed, including the evaluations of costs and benefits within the life cycle of the converter.
6. An energy efficient and reliable auxiliary drive concept has been proposed and assessed using the case study on a vehicular air compressor example.

Practical relevance

The research results cover a set of recommendations and technological improvements for practical application in the auxiliary converter systems of electric vehicles. The outcome of this work corresponds well with the industry demand for cheap, reliable, energy efficient and environmentally friendly solutions in electric vehicle auxiliary converter design requirements. The proposed concepts have been validated experimentally in the laboratory environment and, hence, can be further developed for the testing in the application-relevant environment, certification, type approval and release to the market within the next 4 years.

In the scope of the commercialization training program for scientists, CO.LAB, the commercialization potential of the Thesis results has been assessed. As a result, a technology road map has been created, a total addressable market and market opportunities were evaluated, and the first version of the business model has been developed for advancing the technology in the market in collaboration with industry partner JSC Riga Electric Machine Building Works.

Approbation of research results

In total, 14 publications were created, with 11 publications being presented in the Doctoral Thesis. The approbation and practical relevance of the research results is covered in the following publications:

1. Kondratieva, L., **Bogdanovs, A.**, Overianova, L., Riabov, I., Goolak, S. Determination of the Working Energy Capacity of the On-Board Energy Storage System of an Electric Locomotive for Quarry Railway Transport during Working with a Limitation of Consumed Power. *Archives of Transport*, 2023, Vol. 65, No. 1, pp. 119–136. ISSN 0866-9546. e-ISSN 2300-8830. Available from: doi:10.5604/01.3001.0016.2631

2. **Bogdanovs, A.**, Krievs, O., Pforr, J. Wide Bandgap SiC and GaN Semiconductor Performance Evaluation in a 3-Phase 3-Level NPC Inverter for Transportation Application. In: *2022 IEEE 63rd International Scientific Conference on Power and Electrical Engineering of Riga Technical University (RTUCON 2022): Conference Proceedings*, Latvia, Riga, 10–12 October 2022. Piscataway: IEEE, 2022, pp. 301–307. ISBN 978-1-6654-6559-5. e-ISBN 978-1-6654-6558-8. Available from: doi:10.1109/RTUCON56726.2022.9978767

3. Klints, A., **Bogdanovs, A.**, Zarembo, J. FEA Based Traction Converter Thermal Design Method for Railway Application Using Mission Profile Definition. In: *2022 IEEE 63rd International Scientific Conference on Power and Electrical Engineering of Riga Technical University (RTUCON 2022): Conference Proceedings*, Latvia, Riga, 10–12 October 2022. Piscataway: IEEE, 2022, pp. 74–80. ISBN 978-1-6654-6559-5. e-ISBN 978-1-6654-6558-8. Available from: doi:10.1109/RTUCON56726.2022.9978854

4. **Bogdanovs, A.**, Vonda, Ē., Grīslis, A., Gailis, M., Zalcmanis, G., Kreicbergs, J. E-Mobility Courses Design for Automotive Engineering Curricula: a Case Study. In: *2022 IEEE 63rd International Scientific Conference on Power and Electrical Engineering of Riga Technical University (RTUCON 2022): Conference Proceedings*, Latvia, Riga, 10–12 October 2022. Piscataway: IEEE, 2022, pp. 7–12. ISBN 978-1-6654-6559-5. e-ISBN 978-1-6654-6558-8. Available from: doi:10.1109/RTUCON56726.2022.9978797

5. **Bogdanovs, A.**, Bubovich, A., Galkin, I. Interdisciplinary Project-based Learning Approach Implementation for Undergraduate Electrical Engineering Students. In: *IEEE 63rd International Scientific Conference on Power and Electrical Engineering of Riga Technical University (RTUCON 2022): Conference Proceedings*, Latvia, Riga, 10–12 October 2022. Piscataway: IEEE, 2022, pp. 116–122. ISBN 978-1-6654-6559-5. e-ISBN 978-1-6654-6558-8. Available from: doi:10.1109/RTUCON56726.2022.9978862

6. **Bogdanovs, A.**, Krievs, O., Pforr, J. Fault-Tolerant Operation Algorithm for a Multi-Phase DC Converter with Coupled Inductors. In: *PCIM Europe Proceedings*, Germany, Nuremberg, 10–12 May 2022. Berlin; Offenbach: VDE VERLAG

GMBH, 2022, pp. 506–515. ISBN 978-3-8007-5822-7. Available from: doi:10.30420/565822070

7. **Bogdanovs, A.**, Krievs, O., Pforr, J. Fault Detection using Indirect DC Link Current Measurement Technique in Multiphase DC Converter with Coupled Inductor. In: *2021 23rd European Conference on Power Electronics and Applications (EPE'21 ECCE Europe): Conference Proceedings*, Belgium, Ghent, 6–10 September 2021. Piscataway: IEEE, 2021, pp. 2890–2899. ISBN 978-1-6654-3384-6. e-ISBN 978-9-0758-1537-5.

8. **Bogdanovs, A.**, Kucajevs, J., Steiks, I., Vītols, K., Zemīte, L., Krievs, O., Leibčs, R. Opportunity Analysis of Battery Electric Vehicle Fast Charging Infrastructure Development in Latvia. In: *2021 IEEE 62nd International Scientific Conference on Power and Electrical Engineering of Riga Technical University (RTUCON 2021): Conference Proceedings*, Latvia, Riga, 15–17 November 2021. Piscataway: IEEE, 2021, pp. 324–331. ISBN 978-1-6654-3805-6. e-ISBN 978-1-6654-3804-9. Available from: doi:10.1109/RTUCON53541.2021.9711718

9. **Bogdanovs, A.**, Krievs, O., Pforr, J. Indirect Multiple DC Link Current Sensing Using Op-Amp Circuits in a Three-Phase Three-Level PWM Inverter. In: *International Exhibition and Conference for Power Electronics, Intelligent Motion, Renewable Energy and Energy Management: Proceedings. Vol. 1*, Germany, Nuremberg, 3–7 May 2021. Berlin; Offenbach: Mesago PCIM GmbH, 2021, pp. 1614–1621. ISBN 978-3-8007-5515-8.

10. **Bogdanovs, A.**, Krievs, O., Ribickis, L., Pforr, J. Fuzzy Logic Current Balancing Controller Implementation in an Automotive Multi-Phase DC Converter with Coupled Inductors. In: *2020 IEEE 61st International Scientific Conference on Power and Electrical Engineering of Riga Technical University (RTUCON 2020): Conference Proceedings*, Latvia, Riga, 5–7 November 2020. Piscataway: IEEE, 2020, Article number 9316473. ISBN 978-1-7281-9511-7. e-ISBN 978-1-7281-9510-0. Available from: doi:10.1109/RTUCON51174.2020.9316473

11. **Bogdanovs, A.**, Krievs, O., Pforr, J. Indirect DC Link Current Measurement Technique Using an Op-Amp Circuit in an Automotive DC Converter with Coupled Inductors. In: International Exhibition and Conference for Power Electronics, Intelligent Motion, Renewable Energy and Energy Management: Proceedings. Vol. 1, Germany, Nuremberg, 7–8 July 2020. Berlin; Offenbach: Mesago PCIM GmbH, 2020, pp. 60–67. ISBN 978-3-8007-5245-4. ISSN 2191-3358.

INTRODUCTION

The demand for auxiliary converter power in transportation applications is increasing, and this requires more complex solutions and novel approaches for auxiliary power supply design. As discussed in [1], the drawn auxiliary system power in trolleybuses has become so high that it is challenging to provide an acceptable supply during momentary power interruptions due to travelling through insulated grid sections. A typical functional diagram of a trolleybus electric power circuit is shown in Fig. 1 [2]. Another example is the functional diagram of an electric locomotive power circuit, depicted in Fig. 2 [3].
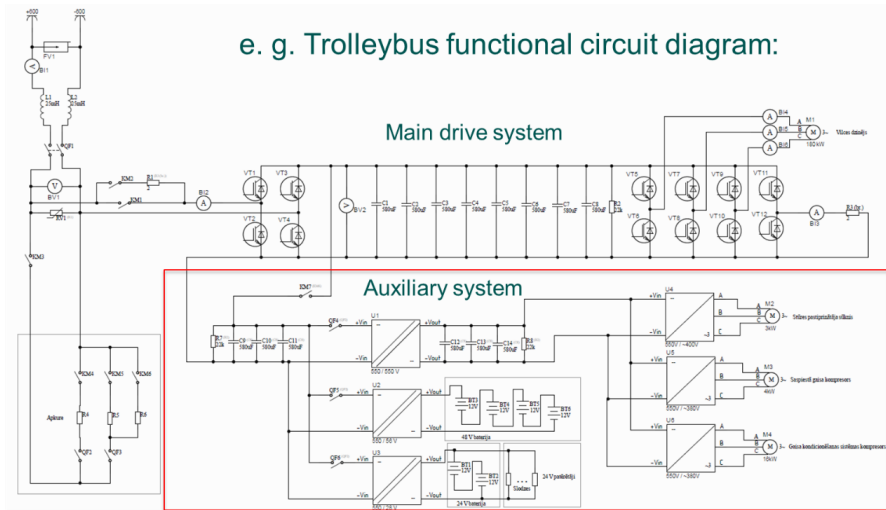
Fig. 1. Example of a functional diagram of a typical trolleybus electric power circuit.
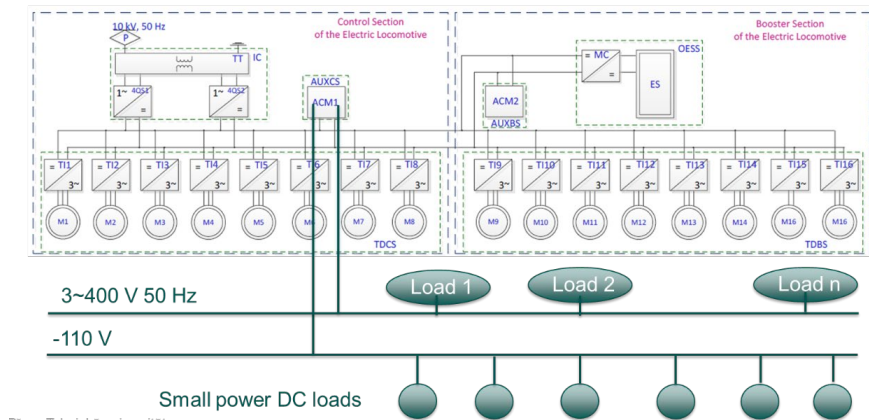
Fig. 2. Example of the functional diagram a railway locomotive power circuit.

As seen in Figs. 1 and 2, the diagram consists of the main drive system and the auxiliary system. The auxiliary system can be divided into 2 major parts – small loads supplied from the DC system and large loads and auxiliary drives supplied by the AC system. The rising auxiliary system power demand trends require higher power ratings and increased efficiency in auxiliary converters, but currently, increasing the converter weight and dimensions or installing multiple converters in parallel is seen as the main solution. Another problem arises in the DC system supply for many relatively small loads. As there is a large number of DC loads with unpredictable mission profiles, the voltage regulation problem arises, and this requires innovative solutions for the DC converter design and control to ensure a very dynamic power supply. A single DC/AC inverter is used to supply a finite number of loads with relatively large power drawn from the AC system. In case of the simultaneous load turn-on, an overcurrent or overload due to the transients might happen. Moreover, in case of a converter failure the whole AC system, including safety critical loads, will fail. Finally, the conservative design of the auxiliary system supply leads to low efficiency, wasted energy, and very dynamic load characteristics, leading to thermal cycling, shorter component lifetime, and less reliable operation.

The largest part of auxiliary power is consumed by auxiliary drives, i.e., power steering, air compressor and air conditioning system. Hence, an optimization of these systems is the most reasonable. In [4], a permanent magnet synchronous machine is proposed to increase the efficiency and reliability of a 6-kW auxiliary oil pump, requiring a variable frequency drive supply. Similarly, in [5], integrated variable frequency drives are recommended for propulsion and auxiliary system drives to achieve high efficiency, reduced weight, and compact design. According to the case study in [6], the multi-level inverter topology realized with wide bandgap semiconductors can offer excellent performance, which is essential for variable frequency auxiliary system drives in transportation applications. Consequently, the multi-level DC/AC inverter realized with SiC or GaN semiconductors can be considered an optimal solution.

An effective solution for the non-isolated DC/DC auxiliary converter with high requirements for dynamic performance is the multiphase bidirectional buck converter with coupled inductor topology. Multi-phase DC converters are widely used in different applications, as their interleaved operation principle ensures high efficiency and low output current ripple compared to single phase converters [7]–[24]. Multi-phase bi-directional buck converters meet the requirements for automotive application, where different voltage levels must be interconnected with improved dynamic performance and no galvanic isolation is required between input and output [7]–[10]. The multi-phase converters with coupled inductors ensure even a better solution because they provide even higher efficiency, low phase current ripples, compact design due to reduced inductor core volume, and high energy density [7]–[13] [23] [24]. However, a big issue of coupled inductor converters is a necessity of phase current balancing controller implementation, as even slight differences in inductor volt-second products cause significant phase current misbalance, leading to efficiency decrease, enlarged current and voltage ripples, inductor core saturation, and even converter failure [10]. Hence, the differences between all phase inductor currents must be determined and controlled to operate the converter efficiently and avoid system failure.

1. SENSING AND MEASUREMENT IN AUXILIARY CONVERTERS

Sensing and measurement techniques play a crucial role in auxiliary converters. To design an intelligent and reliable control system, the main converter parameters, i.e. voltage and current, must be determined or estimated. This chapter describes the general approach for cost-effective and reliable current-sensing techniques for multi-phase converters using single sensor and introduces the novel Indirect Current Measurement (ICM) technique that can be used in multi-phase DC/DC converters and DC/AC inverters.

1.1. General approach for current measurement using single sensor

Implementing a separate current sensor for each converter phase would be a very expensive solution [11]–[13]. In [20], a single sensor scheme is proposed; however, additional switches are required to perform measurements. In [14]–[16], sensorless current sharing techniques are described, but in [15] and [18] significant errors are shown between the phase current values, and in [14], slow transient response is shown. Therefore, recently a lot of attention has been paid to single current sensor schemes deploying the DC-link current measurement with the following phase-current reconstruction algorithms [11]–[13], [17]–[20]. It is shown in [11]–[13], that the current sharing based on single DC link current sensor measurements is possible in coupled inductor converters with small errors and good transient behaviour.

As shown in [4], the DC link current can be mathematically represented by Eq. (1.1) as the sum of the phase current and the pulse width modulation (PWM) switching function products. The PWM switching function is represented by Eq. (1.2). Considering Eqs. (1.1) and (1.2), in an interleaved N-phase converter, phases are shifted by T/N, therefore, the DC link current may contain the sum of 0 up to N phase currents depending on the duty cycle range and, hence, N duty cycle ranges must be analysed. From measurements of the DC link current at each phase, PWM carrier valley, and peak points, the corresponding sum of phase currents is obtained [7]. These results are then represented by Eqs. (1.3) and (1.4), respectively, where A_{vi} and A_{pi} are N × N matrices.

$$I_{DC}(t) = \sum_{i=1}^{N} I_i(t) \cdot S_i(t), \tag{1.1}$$

where I_i is phase current, A, and S_i is the PWM switching function.

$$S_i(t) = \begin{cases} 1 \ if \ 0 + \varphi_i < t < D_i \cdot T + \varphi_i \\ 0 \ if \ D_i \cdot T + \varphi_i < t < T + \varphi_i, \end{cases} \tag{1.2}$$

where φ_i is phase shift, s; T is the PWM switching period; and D_i is the duty cycle.

$$\begin{bmatrix} I_{v1} \\ \vdots \\ I_{vN} \end{bmatrix} = \overline{A_v} \cdot \begin{bmatrix} I_1 \\ \vdots \\ I_N \end{bmatrix}, \tag{1.3}$$

where I_{vi} is measurement of the DC link current at the i-phase of PWM carrier valley point, A, and $\overline{A_v}$ is the current reconstruction matrix of PWM carrier valley points.

$$\begin{bmatrix} I_{p1} \\ \vdots \\ I_{pN} \end{bmatrix} = \overline{A_p} \cdot \begin{bmatrix} I_1 \\ \vdots \\ I_N \end{bmatrix},$$ (1.4)

where I_{pi} is measurement of the DC link current at the i-phase of the PWM carrier peak point, A, and $\overline{A_p}$ is the current reconstruction matrix of the PWM carrier peak point.

The dependency between the PWM carriers and the current waveforms with DC link current sensing solution is shown in the 3-phase converter example for 3 duty cycle ranges in (Fig. 1.1).
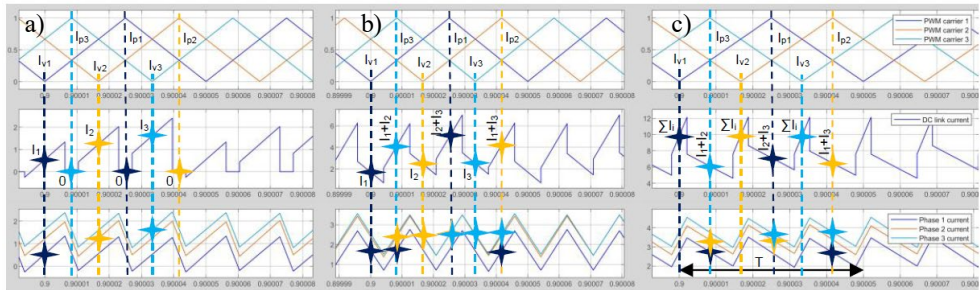
Fig. 1.1. Current waveforms of a 3-phase converter: a) D < 1/3; b) 1/3 < D < 2/3; c) D > 2/3.

Current reconstruction algorithms are derived for each duty cycle range by inversing the matrices A_{vi} and A_{pi} and, hence, the phase current average values are obtained from the DC link current measurements. The limitations of the proposed method arise when any of the matrices A_{vi} or A_{pi} becomes singular. This happens if they consist of zeros or ones, or the number of summed phase currents in the corresponding DC link current measurements has the same multiplier as the converter number of phases N. Hence, the limitations occur only in converters with composite number of phases N within separate duty cycle ranges. Thus, for the converters with a prime number of phases, a general approach can be specified, as shown in (Fig. 1.2).

Duty cycle range		0…1/N	1/N…2/N	2/N…3/N	…	(N-3)/N…(N-2)/N	(N-2)/N…(N-1)/N	(N-1)/N…1
Number of summed phase currents at DC link current measurement from…	valley	1	1	3	…	N-2	N-2	N
	peak	0	2	2	…	N-3	N-1	N-1
Reconstruction algorithm from measurements at…	valley	algorithm 1	algorithm 1	alg. 3	…	algorithm N-2	algorithm N-2	-
	peak	-	algorithm 2	algorithm 2	…	alg. N-3	algorithm N-1	algorithm N-1

Fig. 1.2. General approach to DC link current sensing and phase current reconstruction.

The performed current waveform analysis shows a clear dependency between the DC link and the phase current waveforms. For the converters with prime number of phases, single DC link current sensor measurements can be used for phase current reconstruction within the whole duty cycle range. For the converters with composite number of phases, the limitations of duty cycle ranges will occur when using a single sensor, or a reduced number of DC link current sensors can be used to ensure operation within the whole duty cycle range. The described

current measurement concept is valid for multi-phase uncoupled and coupled inductor converters with any number of phases. The corresponding publication is in Appendix 1.

1.2. Indirect current measurement in multi-phase DC converter

The previously described DC link current measurements were performed directly [11]–[13] because the converter contains only one DC link capacitor with a sensor position between the DC link and the half-bridges, as shown in (Fig. 1.3 a)). However, if the sensor position is changed, as shown in (Fig. 1.3 b)), the DC link current must be obtained indirectly. The DC link current is obtained indirectly using capacitor voltage by means of Eq. (1.5).

$$I_s = I_{s1} + I_{s2} \ldots + I_{sN} = I - I_C = I - C\frac{dV_C}{dt}, \tag{1.5}$$

where

I_s – DC link current, A;

I_{si} – current flowing into i-half-bridge, A;

C – DC link capacitance, F;

V_C – DC link capacitor voltage, V.

a)   b)
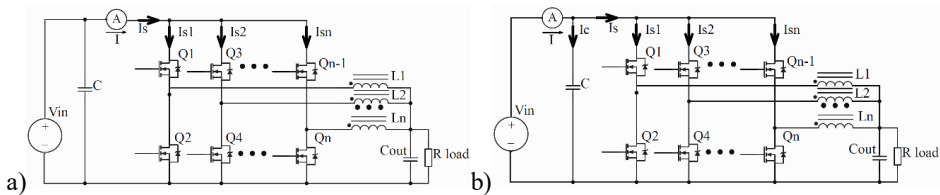
Fig. 1.3. Multi-phase converter with coupled inductors and a) the previously in [9]–[11] used sensor position; b) the proposed sensor position together with the capacitor current determined by capacitor voltage measurement.

In low voltage converters, where metal–oxide–semiconductor field-effect transistors (MOSFETs) with low on-state resistance and breakdown voltage are used, the path length between the half-bridge switches and the capacitor must be kept minimal to avoid transient overvoltage caused by path parasitic inductance. To achieve that, an installation of capacitors, located near each of the half-bridges, would be suggested. Thus, a multi-phase converter with multiple distributed DC link capacitors is obtained, as in Fig. 1.4) The DC link current for a 5-phase converter can be expressed by Eq. (1.6), considering the current sensor measurement and currents flowing into the distributed DC link capacitors. Rearranging Eq. (1.6) for capacitor voltages gives Eq. (1.7):

$$I_s = I_{s1} + I_{s2} + I_{s3} + I_{s4} + I_{s5} = -I - I_{c1} - I_{c2} - I_{c3} - I_{c4} - I_{c5}, \tag{1.6}$$

where I_{ci} is the current flowing into the i-distributed DC link capacitor, A.

$$I_s = -I - C_1\frac{dV_{c1}}{dt} - C_2\frac{dV_{c2}}{dt} - C_3\frac{dV_{c3}}{dt} - C_4\frac{dV_{c4}}{dt} - C_5\frac{dV_{c5}}{dt}, \tag{1.7}$$

where C_i is the distributed DC link i-capacitance, F, and V_{ci} is the distributed i-DC link voltage, V.

A summing of the differential amplifier circuit is designed, based on Eq. (1.8), considering the reverse direction of the input current sensor. Additionally, an offset voltage for bidirectional current sensing and internal PT_1 performance is included by adding capacitor C17 in the feedback loop. Applying Kirchhoff's Current Law to the inverting input and considering the current sensor winding ratio gives Eq. (1.8) for an op-amp circuit output signal:

$$C_{17}\frac{dV_{sig}}{dt} + \frac{V_{sig}}{R_6} = \frac{V_s}{R_2} + I \cdot \frac{N_1}{N_2} \cdot \frac{R_1}{R_1+R_3} - C_6\frac{dV_{c1}}{dt} - C_7\frac{dV_{c2}}{dt} -$$
$$-C_8\frac{dV_{c3}}{dt} - C_9\frac{dV_{c4}}{dt} - C_5\frac{dV_{c5}}{dt}, \qquad (1.8)$$

where

V_{sig} – operational amplifier output voltage, V;

$\frac{N_1}{N_2}$ – the Hall effect current sensor winding ratio;

$C_i - i$-capacitance, F;

$R_i - i$-resistance, Ω.

To increase an op-amp circuit's immunity against common and differential mode disturbances, it is designed as a fully symmetric differential amplifier and additionally, a small output low-pass filter is applied, consisting of R8 and C18. Thus, a filtered signal is obtained, representing the restored DC link current waveforms. The obtained signal can now be used by the ADC converter for DC link current measurement and phase current reconstruction, as described in Section 1.1.
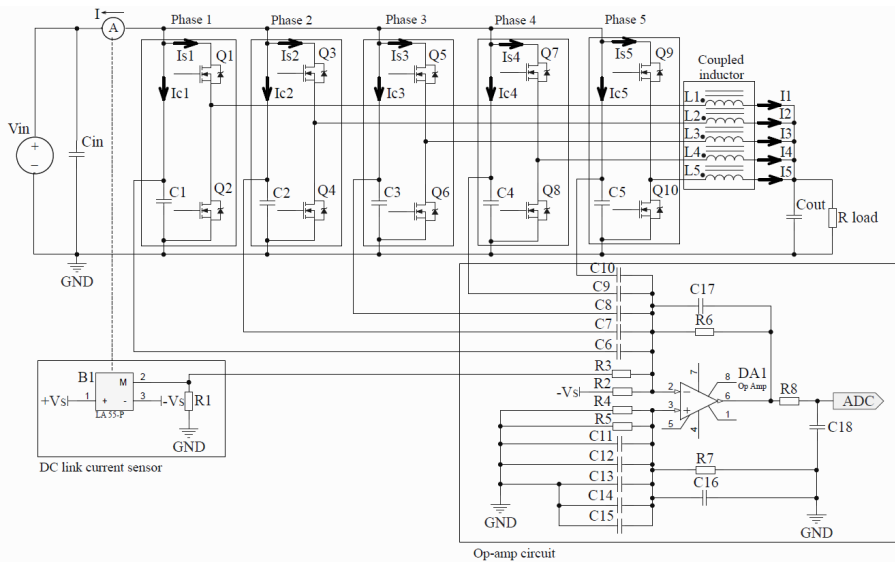
Fig. 1.4. The investigated 5-phase converter with coupled inductor circuit diagram with an operational amplifier circuit for indirect current sensing.

The proposed concept of ICM has been validated experimentally. Firstly, the indirectly acquired DC link current waveforms are compared with the phase current waveforms under normal operating conditions. The cases with balanced and unbalanced phase currents are shown

15

in Figs. 1.5 a), b), respectively. In the first case, phase currents are almost equal and therefore, the restored DC link current waveform is lined up with sampled values nearly the same. In case of misbalance, the phase currents are unequal and the signal obtained from the op-amp circuit reflects an existing phase current misbalance. Secondly, the current measurement accuracy is investigated. The differences between the reconstructed and measured phase current values are compared at different converter operating points within the whole duty cycle range. The resulting deviations are shown in Fig. 1.6. The accuracy of the proposed method is adequate, the phase current misbalance is well represented by the ICM sensing signal and the measurement error is well below 0.5 A in the wide operation range. For more details, refer to [25].
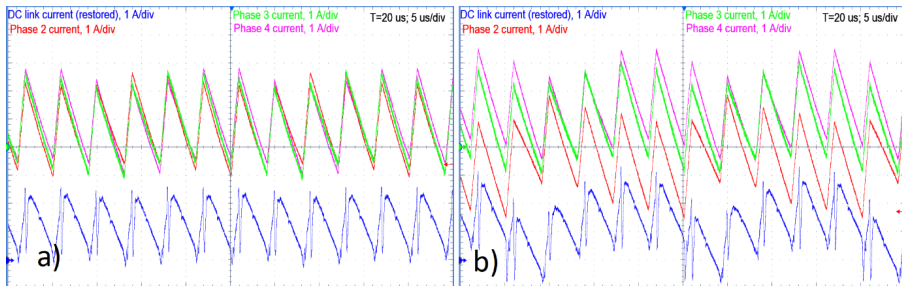
Fig. 1.5. Converter current waveforms under normal operating conditions in cases of a) balanced and b) unbalanced phase currents.
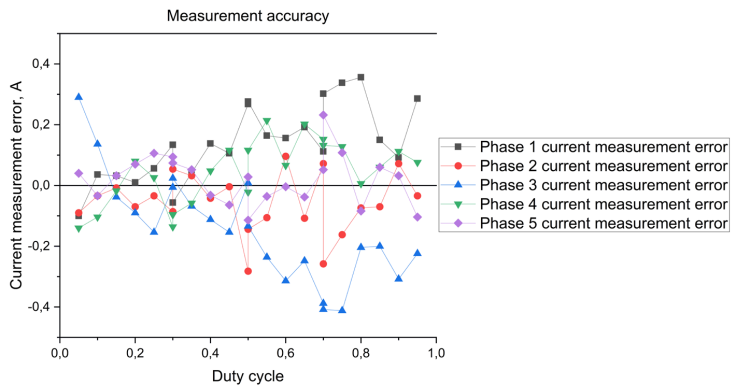
Fig. 1.6. Deviations between measured and reconstructed phase current values.

1.3. Indirect current measurement in multi-level inverter

The dependency between the DC link and phase currents in inverters has been investigated in [26]–[35]. Hence, the indirect measurement approach can be extended for a multi-level inverter with planar busbars between DC link capacitors and switching devices, by placing an input current sensor at the positive DC rail. Additionally, 2 operational amplifier circuits are

implemented to restore the top (TDC) and neutral (NDC) DC link current waveforms, thus, ensuring indirect fault tolerant multiple DC link current sensing (MDCS) [26]–[29] by means of single sensor and sensorless sensing techniques, respectively. The indirect multiple DC link current sensing (MDCS) technique is analysed on a 3-phase 3-level neutral point diode clamped PWM inverter example, which is shown in Fig.1.7, with the corresponding operational amplifier circuits used for DC link current waveform restoration. Using Fig. 1.7, the top and neutral DC link currents can be expressed by Eqs. (1.9) and (1.10).

$$I_{TDC} = -I_{in} - I_{C1} = -I_{in} - C_1 \frac{dV_{C1}}{dt}, \qquad (1.9)$$

where

I_{c1} – current flowing into the top DC link capacitor, A;

I_{in} – input current at the positive rail, A;

C_1 – top DC link capacitance, F;

V_{c1} – top DC link voltage, V.

$$I_{NDC} = I_{C1} - I_{C2} = C_1 \frac{dV_{C1}}{dt} - C_2 \frac{dV_{C2}}{dt}, \qquad (1.10)$$

where

I_{c2} – the current flowing into the bottom DC link capacitor, A;

C_2 – bottom DC link capacitance, F;

V_{c2} – bottom DC link voltage, V.
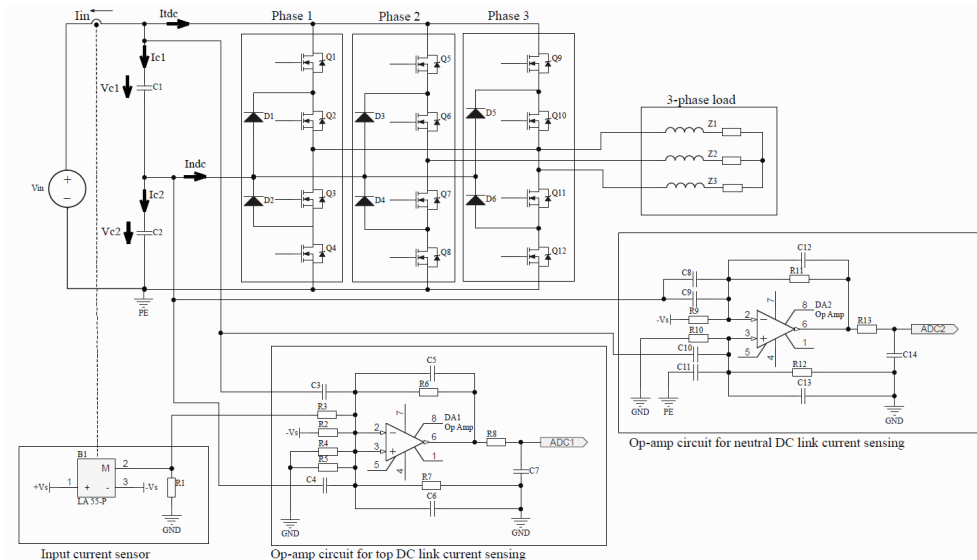
Fig. 1.7. Investigated 3-phase 3-level neutral point diode clamped inverter circuit diagram with 2 operational amplifier circuits for indirect current sensing.

The proposed concept of ICM has been validated experimentally. Firstly, the correspondence of current waveforms between experimental and simulation results for a switching frequency of 2 kHz is shown in (Fig. 1.8). The calculated TDC and NDC waveforms are preserved by the op-amp circuits. Separately reconstructed phase current values are shown in (Fig. 1.9). An example phase current reconstruction outcome for the 5 kHz switching frequency is shown in (Fig. 1.10).
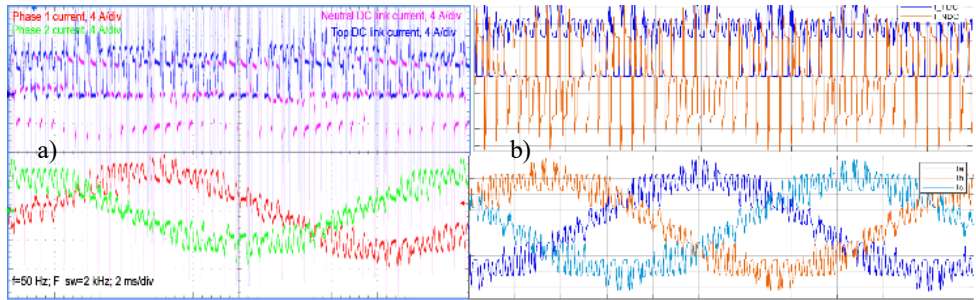
Fig. 1.8. a) Experimental and b) simulated inverter current waveforms at a 2 kHz switching frequency.
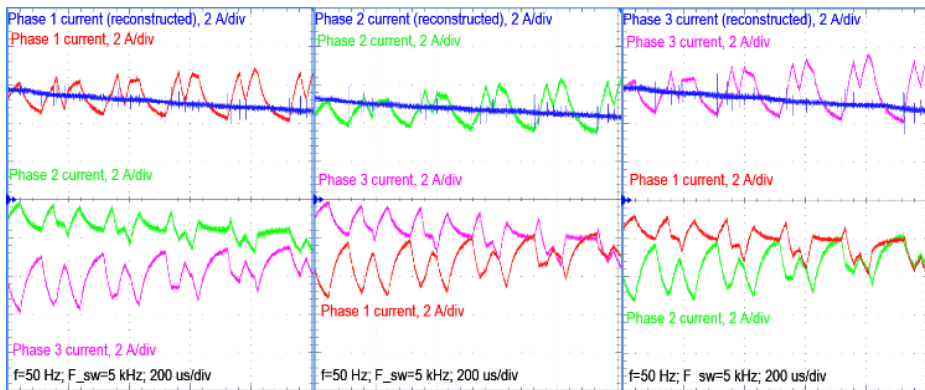
Fig. 1.9. Separately reconstructed phase currents.
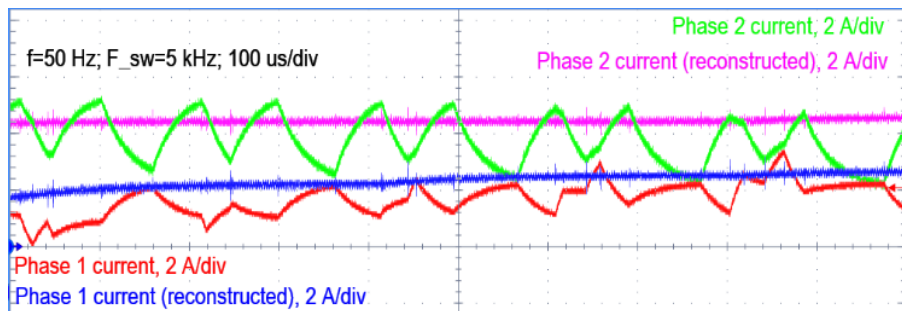
Fig. 1.10. Phase current reconstruction at a 5 kHz switching frequency.

The indirect MDCS has shown good current waveform quality, high precision and immunity against disturbances. Further analysis of TDC and NDC current samples, by evaluating the difference between reconstructed and real phase current values, has shown, that the indirect DC link current sensing technique achieves an adequate measurement accuracy. The precision of acquired current measurements is mainly influenced by signal filtering, differences between phase-to-phase impedances, passive component tolerances, DC link capacitor ESR, and correct measurement window setup. With inverter switching frequencies up to 20 kHz, the reconstructed phase current value maximum measured deviation at separate points did not exceed 20 %. At most of the acquired measurement points (> 90 %), the relative error was below 10 %. The achieved accuracy was lower at high switching frequencies and gradually improved with the frequency decrease. Hence, the indirect MDCS can be used in modern power supply and electrical drive applications. Moreover, it can be extended for multi-phase and multi-level inverters. A more detailed analysis is given in [36].

1.4. Conclusions

The dependency between the DC link and phase current waveforms can be used for cost-effective single-sensor measurements. For converters with a prime number of phases, single DC link current sensor measurements can be used for phase current reconstruction within the whole duty cycle range. For converters with a composite number of phases, the limitations of duty cycle ranges will occur when using a single sensor, or a reduced number of DC link current sensors can be used to ensure operation within the whole duty cycle range.

Using an indirect DC link current measurement technique for a multi-phase DC converter with coupled inductors, the DC link current waveforms can be restored in good quality using a single current sensor with an operational amplifier circuit in converters with distributed DC link capacitors. The accuracy of the proposed ICM method in multiphase DC/DC converters is adequate, phase current misbalance is well represented by the ICM sensing signal and the measurement error is well below 0.5 A in the wide operation range. Achieved precision in real operating conditions is sufficient for a current balancing controller implementation.

The proposed ICM technique is valid for single sensor or sensorless phase current detection in the multi-level inverters, using TDC or NDC sensing separately. The TDC and NDC waveforms can be restored using a single current sensor with 2 operational amplifier circuits, both forming a reliable MDCS technique, used for phase current reconstruction. The indirect MDCS has been verified using simulation and experimental results and has shown good current waveform quality, high precision, and immunity against disturbances. Hence, the indirect MDCS can be used in modern auxiliary power supply and drive applications.

2. AUXILIARY CONVERTER CONTROL

The auxiliary converter controller design is an essential step to achieve the objective of energetically and economically effective technology. To develop an intelligent and reliable control system with fast response, the system's internal parameters and behaviour must be analysed narrowly. This chapter describes the converter system transfer function determination and controller design and analyses the fuzzy logic controller performance under different circumstances. The detailed fuzzy logic controller design is described in [37].

2.1. Coupled inductor analysis

The 5-phase DC/DC converter, considered in Section 1.2, is built as a coupled inductor. The coupled inductor is formed by the differential configuration of 5 toroidal N87 cores EPCOS B64290L0082X087 with 5 turns for each phase winding. The coupled inductor configuration with a superimposed magnetic circuit is shown in (Fig. 2.1). The corresponding magnetic circuit diagram is shown in (Fig. 2.2). The inductance matrix measurement results in the linear range are represented in Eq. (2.1).
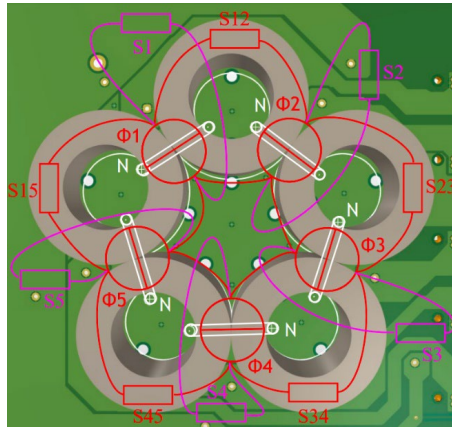
Fig. 2.1. Coupled inductor configuration in a converter.
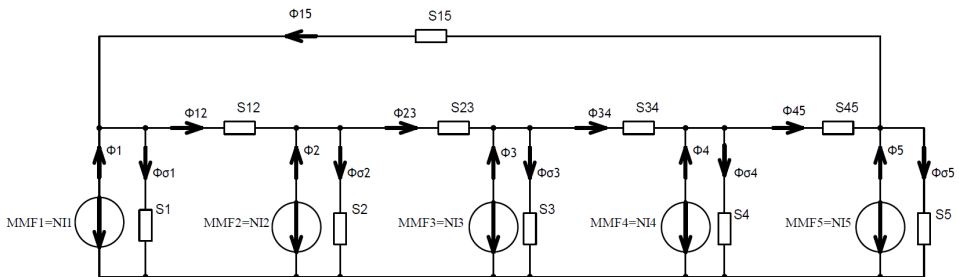
Fig. 2.2. Coupled inductor magnetic circuit.

$$L = \begin{bmatrix} 211 & -104 & 0 & 0 & -106 \\ -104 & 210 & -104 & 0 & 0 \\ 0 & -104 & 209 & -104 & 0 \\ 0 & 0 & -104 & 210 & -104 \\ -106 & 0 & 0 & -104 & 212 \end{bmatrix}, \qquad (2.1)$$

where L is the inductance matrix (in linear range), µH;

The considered coupled inductor magnetic circuit diagram is analysed to obtain the mathematical model for the further non-linear analysis and determination of transfer function. By applying the superposition theorem to the magnetic circuit shown in (Fig. 2.2), Equation system (2.2) is obtained:

$$\begin{cases} \Phi_1 = \Phi_{\sigma 1} + \Phi_{12} - \Phi_{51} = \dfrac{MMF_1}{S_1} + \dfrac{MMF_1}{S_{12}} - \dfrac{MMF_2}{S_{12}} - \dfrac{MMF_5}{S_{51}} + \dfrac{MMF_1}{S_{51}} \\[2mm] \Phi_2 = \Phi_{\sigma 2} + \Phi_{23} - \Phi_{12} = \dfrac{MMF_2}{S_2} + \dfrac{MMF_2}{S_{23}} - \dfrac{MMF_3}{S_{23}} - \dfrac{MMF_1}{S_{12}} + \dfrac{MMF_2}{S_{12}} \\[2mm] \Phi_3 = \Phi_{\sigma 3} + \Phi_{34} - \Phi_{23} = \dfrac{MMF_3}{S_3} + \dfrac{MMF_3}{S_{34}} - \dfrac{MMF_4}{S_{34}} - \dfrac{MMF_2}{S_{23}} + \dfrac{MMF_3}{S_{23}} \\[2mm] \Phi_4 = \Phi_{\sigma 4} + \Phi_{45} - \Phi_{34} = \dfrac{MMF_4}{S_4} + \dfrac{MMF_4}{S_{45}} - \dfrac{MMF_5}{S_{45}} - \dfrac{MMF_3}{S_{34}} + \dfrac{MMF_4}{S_{34}} \\[2mm] \Phi_5 = \Phi_{\sigma 5} + \Phi_{51} - \Phi_{45} = \dfrac{MMF_5}{S_5} + \dfrac{MMF_5}{S_{51}} - \dfrac{MMF_1}{S_{51}} - \dfrac{MMF_4}{S_{45}} + \dfrac{MMF_5}{S_{45}} \end{cases}, \qquad (2.2)$$

where

$\Phi_{\sigma i}$ – magnetic flux in the air across i-phase windings, Wb;

Φ_{ij} – magnetic flux in the torus between i- and j-phase windings, Wb;

Φ_i – magnetic flux corresponding to i-phase windings, Wb;

MMF_i – magnetomotive force across i-phase windings, A (Ampere-turns);

S_i – reluctance of the air path across i-phase windings, H^{-1};

S_{ij} – reluctance of the toroid between i- and j-phase windings, H^{-1}.

Rearranging Eq. (2.2) to the state space representation gives Eq. (2.3) that can be further used in a simulation model.

$$\begin{bmatrix} \Phi_1 \\ \Phi_2 \\ \Phi_3 \\ \Phi_4 \\ \Phi_5 \end{bmatrix} = \begin{bmatrix} (\frac{1}{S_1}+\frac{1}{S_{51}}+\frac{1}{S_{12}}) & -\frac{1}{S_{12}} & 0 & 0 & -\frac{1}{S_{51}} \\[2mm] -\frac{1}{S_{12}} & (\frac{1}{S_2}+\frac{1}{S_{12}}+\frac{1}{S_{23}}) & -\frac{1}{S_{23}} & 0 & 0 \\[2mm] 0 & -\frac{1}{S_{23}} & (\frac{1}{S_3}+\frac{1}{S_{23}}+\frac{1}{S_{34}}) & -\frac{1}{S_{34}} & 0 \\[2mm] 0 & 0 & -\frac{1}{S_{34}} & (\frac{1}{S_4}+\frac{1}{S_{34}}+\frac{1}{S_{45}}) & -\frac{1}{S_{45}} \\[2mm] -\frac{1}{S_{51}} & 0 & 0 & -\frac{1}{S_{45}} & (\frac{1}{S_5}+\frac{1}{S_{45}}+\frac{1}{S_{51}}) \end{bmatrix} \cdot \begin{bmatrix} MMF_1 \\ MMF_2 \\ MMF_3 \\ MMF_4 \\ MMF_5 \end{bmatrix},$$

$$(2.3)$$

where

Φ_i – magnetic flux corresponding to i-phase windings, Wb;

MMF_i – magnetomotive force across i-phase windings, A (amperturns);

S_i – reluctance of the air path across i-phase windings, H^{-1};

S_{ij} – reluctance of the toroid between i- and j-phase windings, H^{-1}.

For the further non-linear analysis of the coupled inductor behaviour in converter under different ultimate operation conditions, a B-H (magnetization) curve of N87 ferrite is combined with the toroid dimensions. Considering a linear dependency between the reluctance and the magnetic field strength, the resultant magnetic flux dependency on magnetomotive force has been derived and depicted in Fig. 2.3.
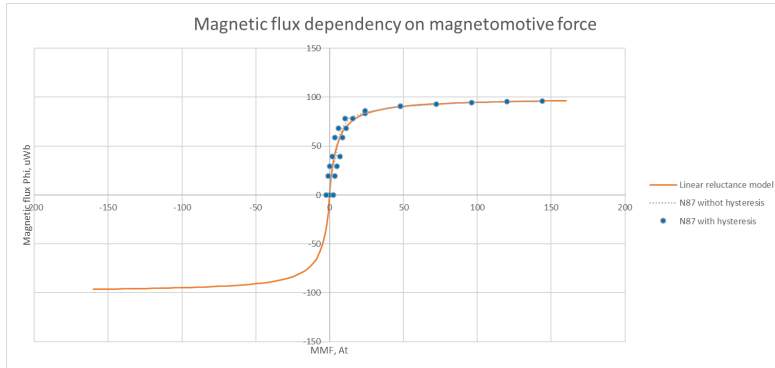
Fig. 2.3. Dependency between the magnetic flux and MMF in a coupled inductor.

The outcomes of the coupled inductor analysis have been combined in a single simulation model that is used as a digital twin of the multi-phase converter with a coupled inductor. The model has been verified by a direct comparison between simulation and experimental results, as depicted in Fig. 2.4. Thereafter, the acquired simulation model is used to model the converter non-linear behaviour, reaction to ultimate operation conditions, and analysis of the inductor saturation effects. The dependency between the converter duty cycle difference, current misbalance, and converter efficiency is shown in Fig. 2.5. Due to the high coupling factor and small leakage path, the DC component of magnetic flux is compensated in mutual inductor cores if the phase currents and, hence, the fluxes in each core are equal [8]. Since even a small change in the inductor volt-second product causes a phase current misbalance, the DC component of magnetic flux emerges and leads the core towards non-linear region and saturation. Once the coupled inductor core starts to operate in non-linear region, the hysteresis effect will intensify and cause increased core iron losses and, hence, lower efficiency of the converter. Therefore, non-linear controller performance is required for effective current sharing among phases.
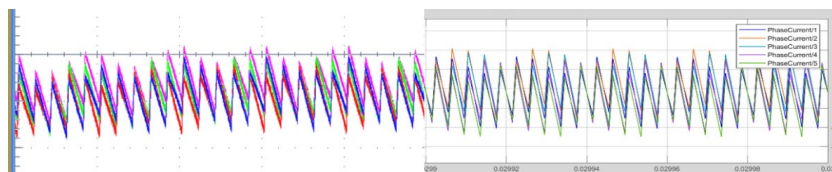
Fig. 2.4. Non-linear simulation model of coupled inductor verification results: experimentally acquired phase currents (left) vs. simulated phase currents (right).
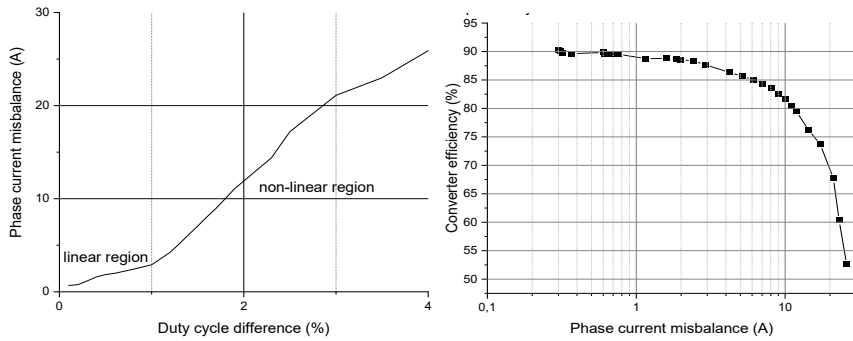
Fig. 2.5. Dependency between the converter duty cycle difference, current misbalance (left),
and converter efficiency (right).

2.2. Fuzzy logic controller design

The control of converter with coupled inductor must consider the non-linear behaviour of the inductor cores, as described in Section 2.1. In addition to that, transient operation at the load change can show undesirable current balancing controller interventions, caused by misbalance due to incorrectly interpreted phase current value change that is a specific issue of single sensor current sharing schemes. The origin of this effect is illustrated in Fig. 2.6. The load increase is shown with the gradually rising phase currents. The sample points of currents are distributed within the switching period, resulting in different values sampled due to the load change and not the misbalance. Nevertheless, a classical balancing controller would try to compensate these different current values, thus causing real phase current misbalance. To overcome these problems a fuzzy logic balancing controller is proposed for the auxiliary DC/DC converter control. The fuzzy logic controller can combine the advantages of non-linear control for MIMO systems, ensuring high performance under varying system dynamics conditions [38]–[41].
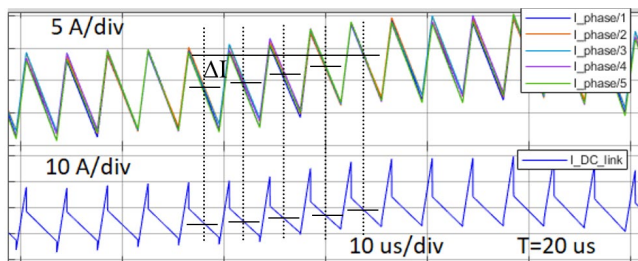
Fig. 2.6. Converter operation at load change illustrating the pseudo-misbalance effect.

The control architecture corresponds to the master-slave topology, where one converter phase is chosen as a master and, hence, an average current in the master phase is used as a reference value. Currents flowing in the rest slave phases are adjusted to a master phase given reference current value. Four identical fuzzy logic controllers are used in master slave current balancing control topology for a 5-phase converter with coupled inductors. Each controller

processes fuzzified current misbalance and load change values at the input and returns a proportional and integral (PI) duty cycle correction at the output. The obtained duty cycle corrections are added to the main duty cycle from the output voltage controller and fed to the corresponding slave phase PWM module. The control architecture is shown in Fig. 2.7.
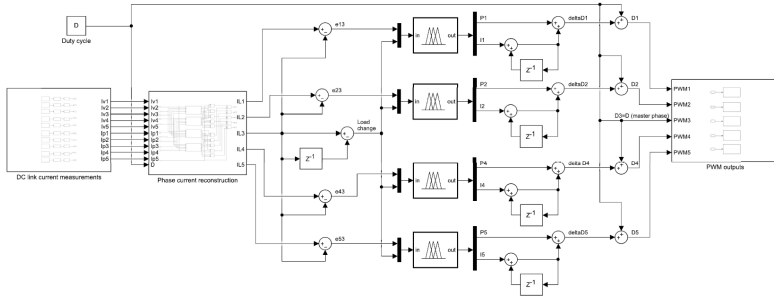
Fig. 2.7. Current balancing control architecture with master-slave topology.

The fuzzy logic controller is designed using Mamdani fuzzy interference system with triangular membership functions for both input (current misbalance and load change) and both output (proportional and integral duty cycle correction) variables. A designed controller architecture with control surfaces for both outputs and 19 control rules are shown in Fig. 2.8.
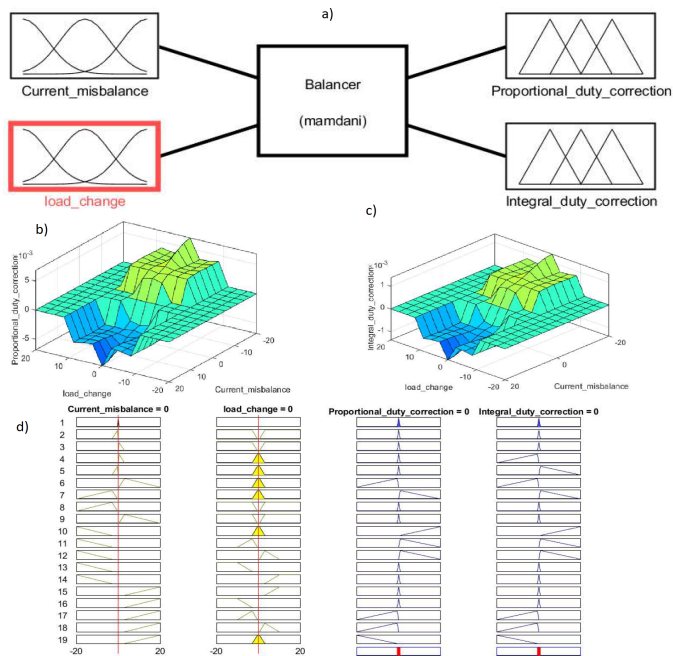
Fig. 2.8. Fuzzy logic controller: a) architecture; b) proportional control surface; c) integral control surface; d) control rules.

2.3. Control performance evaluation

The designed control concept has been validated by simulation and experimentally. Firstly, the comparison between the converter phase currents without and with the turned-on controller at steady state are shown in Fig. 2.9. The phase currents show obvious misbalance with non-linear waveforms, differing from simulation results without the control, but after switching the fuzzy logic current balancing controller on, equal phase currents with linear waveforms are observed in both cases.
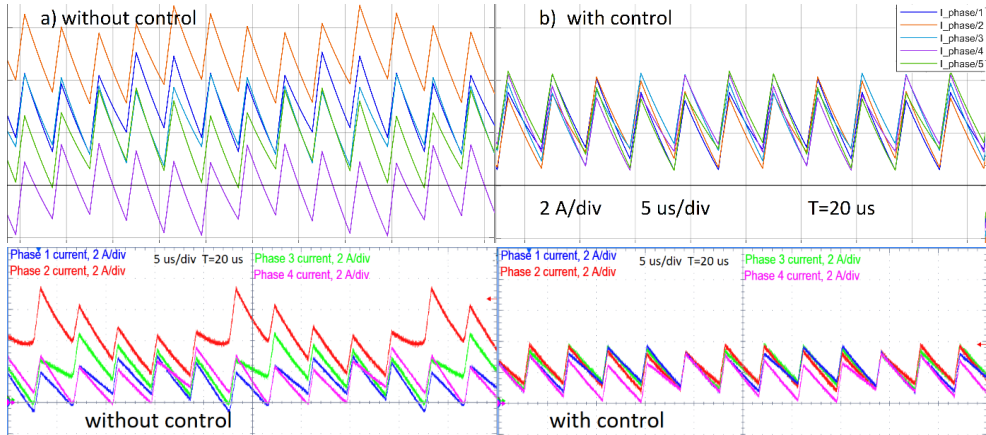
Fig. 2.9. Simulation (top) and experimental (bottom) results for steady state: a) without and b) with current balancing control applied.

The step response of phase current balancing controller is shown by means of phase current waveforms at controller turn-on in Fig. 2.10. The current balancing control can achieve nearly zero steady state error within 1 ms after the controller turn-on, with higher gain initially when prototype converter currents showed stronger misbalance due to core saturation and lower gain in the linear region.
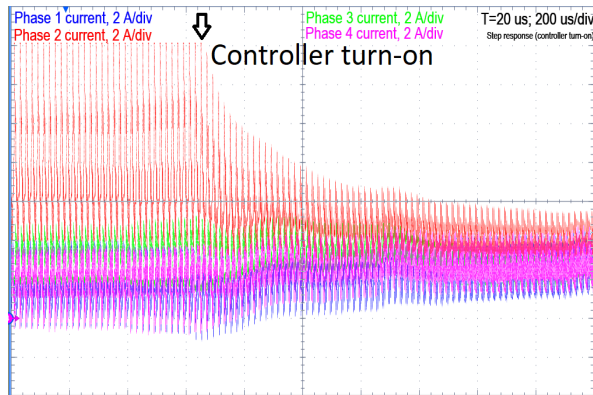
Fig. 2.10. Current balancing controller step response at turn-on.

The phase current waveforms under load current increase conditions are shown in Fig. 2.11 a) and b) without and with load change input variable enabled, respectively. Thus, an influence of load change algorithm on the control performance can be analysed. Significant undesired current balancing control interventions can be observed on phase current waveforms when the load change variable is disabled, and smooth waveforms are observed when the load change algorithm is enabled.
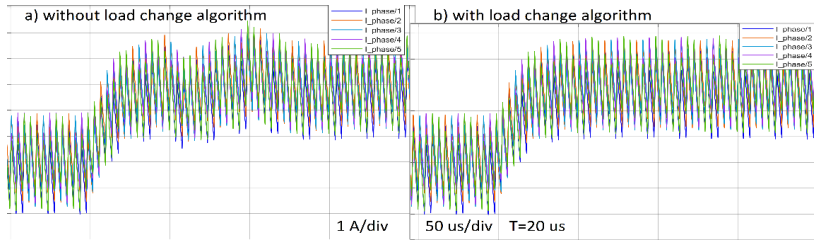
Fig. 2.11. Phase currents at load change: a) without and b) with enabled change algorithm.

Finally, the sinusoidal duty cycle disturbance is applied to measure the controller frequency response. The resultant open loop and closed loop current waveforms are shown in Fig. 2.12. The frequency response for the open and closed loop systems is shown in Fig. 2.13. The open loop system reaction on slow disturbances is large but it decreases for faster disturbances. On the other hand, the closed loop system reaction on slow disturbances is very small, but it gradually increases when disturbance gets faster. Hence, the controller achieves maximum performance on low frequencies, and at high frequencies the control performance is minimal.
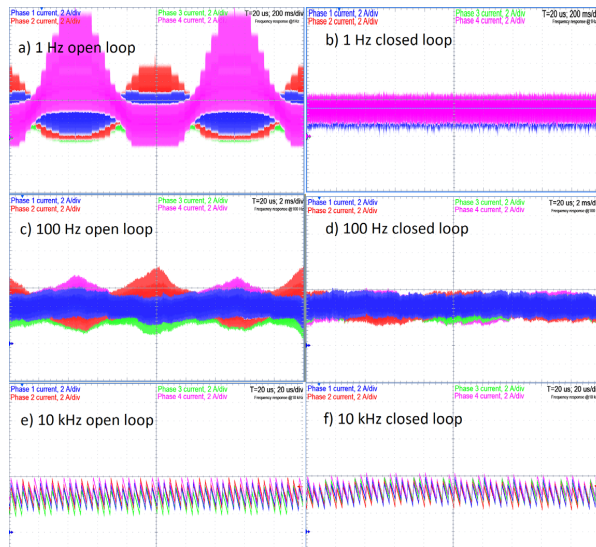
Fig. 2.12. Phase current waveforms under sinusoidal disturbance conditions: a) open loop @ 1 Hz; b) closed loop @ 1 Hz; c) open loop @ 100 Hz; d) closed loop @ 100 Hz; e) open loop @ 10 kHz; f) closed loop @ 10 kHz.
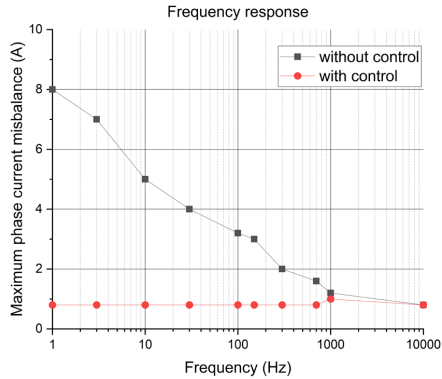
Fig. 2.13. Frequency response on the current misbalance for the open and closed loop.

2.4. Conclusions

Multiphase converter with coupled inductor demonstrates a non-linear behaviour due to the possible core saturation, caused by the current misbalance and resulting magnetic flux DC component. Using the single sensor ICM technique can cause undesired current balancing controller interventions during the load change. Application of fuzzy logic under these circumstances allows to design a non-linear complicated controller in relatively easy and intuitive manner, by measuring the open loop system parameters and applying the cognitive knowledge of the system. As a result, the desired closed loop system behaviour is achieved. The current balancing controller dynamic behaviour was designed to achieve high performance at low frequencies and reduced performance at high frequencies or under fast load change conditions. Simulation and experimental results show good current balancing controller performance at steady state with low steady state error, caused mainly by the ICM circuit accuracy limits. The designed control system can avoid undesirable interventions under load change conditions and provide good dynamic performance of an auxiliary converter.

3. FAULT DETECTION AND FAULT TOLERANCE

Auxiliary converter system provides power supply for safety critical systems. As the failure in power supply may lead to catastrophic consequences, the fault detection and fault tolerant operation is required to ensure reliable uninterruptible power supply. This chapter introduces the converter ICM based fault detection and identification method and describes the fault tolerant operation algorithm for uninterruptible operation even with active fault.

3.1.   Fault detection and identification

As described in the previous chapters, the phase current values can be obtained by means of ICM and used for current mode control or balancing controller implementation, which in both cases will protect the converter from excessive equalizing currents and resulting core saturation and efficiency decrease under normal operating conditions. However, the converter circuit elements, such as semiconductor devices, inductors and capacitors can fail randomly or under certain circumstances [42]. In an automotive bi-directional converter, the MOSFETs have the highest failure risk, resulted by the switch, remaining on short or open circuit state in converter single or multiple phases [42]–[44]. In this case a failure in one or more phases will not lead to the whole converter refusal and, hence, it is essential to determine and locate the fault as quickly as possible, to protect the converter from further damage.

The DC link current waveforms are analysed in terms of failure condition reflection. The ICM technique is used to detect the overall fault conditions and specify the failed component. Fault detection performance is assessed considering the fault type and time necessary for detection. The main distinguishing criteria of normal current misbalance condition is slow appearance and obvious response on current balancing controller interventions. Fault conditions, in opposite, appear suddenly, cause rapid current changes, and do not react to the controller caused duty cycle corrections.

Short circuits are rare, but harmful events [42] causing rapid current rise limited by relatively small parasitic inductances, when both half-bridge switches are closed. Therefore, the short circuit detection must be performed very fast. This can be done by using multiple distributed DC link current measurements within a switching period. Open circuit faults can happen with higher probability but have significantly lower risks of causing permanent converter damage [42]. Nevertheless, open circuit faults must be detected to avoid the rise of equalizing currents, causing coupled inductor saturation. It is generally more challenging to detect open circuit, as it is not always leading to rapid current changes. Hence, the secondary criteria of no reaction on current balancing controller interventions can be used.

Fault detection is based on the reconstructed phase currents from the ICM samples. Phase current average values and their change rates are used for the fault type identification. The overall converter control structure with the failure diagnosis module is depicted by means of a block diagram in Fig. 3.1. The experimental results for four typical fault cases, i.e., high side and low side switch open and short circuit, are shown in Fig. 3.2. In both cases the open circuit

(a) and short circuit (b) conditions are shown with the corresponding digital signal representing the health state that is high for no fault and low for the corresponding fault condition.
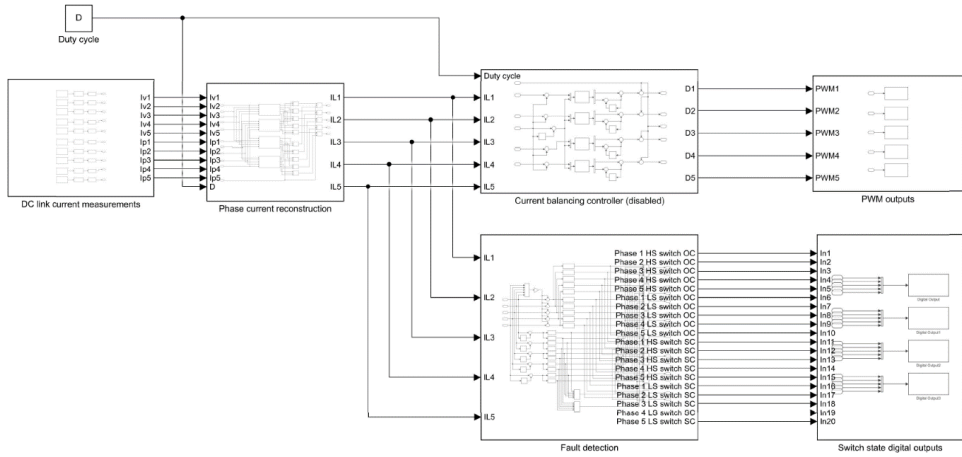
Fig. 3.1. Block diagram of the overall converter control structure including the failure diagnosis module.
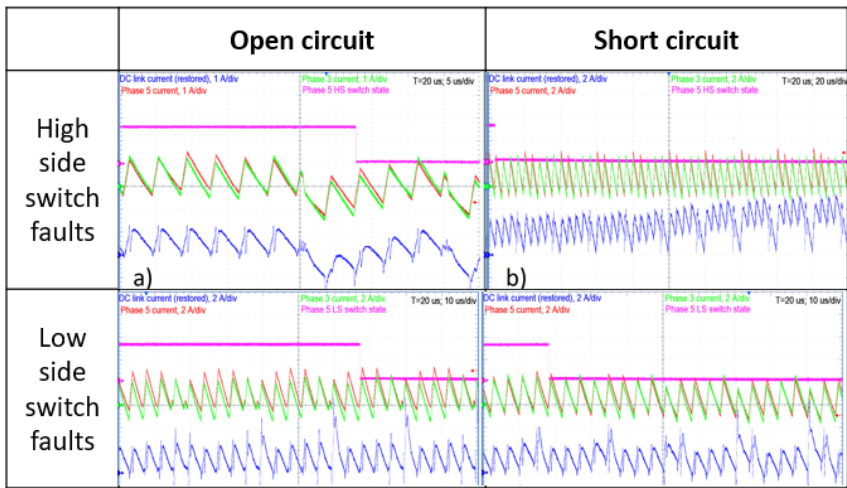
Fig. 3.2. Current waveforms reflecting the specific semiconductor switch faults.

The disturbing factors for fault detection performance might be converter transients and pseudo-fault detection. Converter transient might be caused by sudden load change or rapid input voltage drops. This might lead to pseudo-fault detection when the converter operation is still normal. To overcome this effect, fault detection and identification algorithm includes an additional conditional statement ensuring that the current change is not happening in all phases at the same time. Another pseudo-fault event might happen shortly after the single fault detection event. Especially at short circuit, the converter currents can be exposed to very rapid

changes that might be interpreted by the algorithm as another independent fault event. This drawback can be eliminated only partially, by checking conditional statement, ensuring that the current change is happening only in the affected phase or in the rest phases at the same time.

The fault detection time measurements have been performed to assess the fault detection performance at different converter operating points within the whole duty cycle range. The resulting graph in Fig. 3.3 verifies that the fault state can be detected within 10 to 20 us in the case of open circuit and less than 4 us in the case of short circuit within the whole converter duty cycle range. The switch state estimation utilizes the current change rate and current misbalance evaluation. Hence, the short circuit condition can be detected faster because of higher change rate. Open circuit conditions are generally slower and, therefore, need more time for detection and identification. The more detailed analysis is shown in [45] and [46].
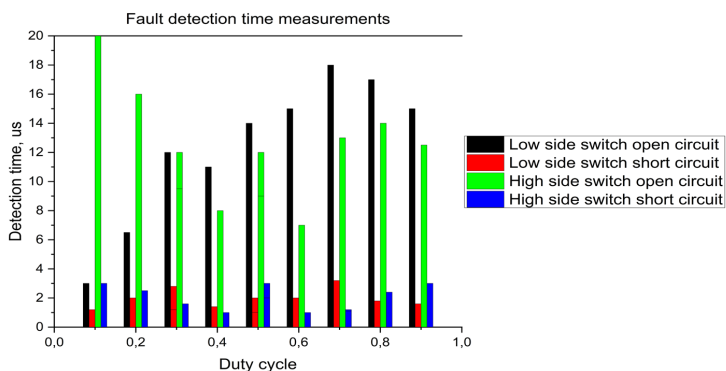
Fig. 3.3. Fault detection time measurements at different converter operation points.

3.2. Fault tolerance

Reliability plays an important role in modern power electronic system design. Recently a concept of Design for Reliability has gained an increased interest for ensuring more reliable and fail-safe field operation of power electronic converters by implementing reliability assessment based on Physics of Failures already at the design stage [47], [48], which is especially important in automotive application [49]. Complete assessment of power electronic system physics of failures requires knowledge about power semiconductors, passive components, control electronics, communication systems, and software wear-out functions, including modelling of thermal cycling, humidity, vibration and other stressors [48]–[50]. The reliability-oriented design of magnetic components challenging [48] in the case of multiphase converter with coupled inductors. Therefore, the use of fault-tolerance concept can be considered to improve and complement the reliability-oriented design by filling the existing gaps in the knowledge and provide fail-safe fault-tolerant operation instead of converter component redundancy.

Fault-tolerance is a key aspect to enhance the power electronic system reliability. Therefore, a lot of research must be conducted on different component degradation mechanisms to minimize the risks of different possible failures [48]–[50]. At some applications (e.g.,

automotive advanced driver assistance and other auxiliary safety-critical systems) black-out of power supply is not an option due to high risks of catastrophic consequences even if the probability of failures is minimized [51]. In this case a system must be able to continue performing its intended function despite the failure [50] or at least provide emergency operation with reduced performance to fulfil the requirements of functional safety [42] as by definition of fault-tolerance. Moreover, the multi-phase design of power electronic converters with fault-tolerant operation algorithm can meet the high standards of functional safety and reduce the component redundancy. Hence, the development of fault-tolerant operation algorithms is essential to provide uninterruptable power supply for safety-critical applications.

Different fault-tolerant operation technics were proposed recently for power electronics systems. A monolithic single-phase integrated circuit with fault detection and switch blocking capabilities is proposed in [51] to ensure fault-tolerance in multi-phase hybrid Dickson converter for safety-critical applications. In [52], an additional inverter leg with four switches is added to a 3-phase inverter to provide fault-tolerant operation of an electric vehicle drive. In [53], the existing buck/buck-boost converter topology is modified with three additional switches to provide a fault-tolerant PV system operation. A boost converter with additional parallel low-side switch is proposed in [54], thus, achieving low side switch interleaved operation in normal mode and single-phase operation in case of the low-side switch open circuit fault. Similarly, a unidirectional interleaved 3-phase boost converter with additional fuses is used for isolation of a faulty phase and ensuring fault-tolerant operation with reduced number of phases [55]. Hence, in most cases additional components are used for redundancy and in case of faults the power flow is distributed between the remaining components. Though, it is an indicator of not optimal component utilization in normal operation (healthy) mode.

Fault-tolerant operation and reliability of bi-directional multi-phase interleaved buck converters was investigated recently and showed good results. Operation of a 4-phase converter with deactivated phases was investigated in [43] and showed a possibility of coupled ladder type core saturation without power loss increase. A partially decentralized control algorithm with PWM carrier phase-shift re-configuration was proposed in [56] and achieved operation with stable output voltage in the case of 4-phase converter with uncoupled inductors and multiple current sensors. Fault tolerant single-phase operation of a 2-phase converter with none, weak, and strong coupling was investigated in [57], achieving better results for the case of weakly-coupled inductors. Reliability indicator comparison is presented in [43], showing the benefits of coupled inductor converters over uncoupled inductor multi-phase and single-phase buck converters. Hence, the multi-phase interleaved buck converter topology utilizing coupled inductors has advantages in terms of reliability, fault-tolerance, and ability to provide fail-safe operation in safety-critical applications.

The proposed fault-tolerant operation algorithm is initiated in case of an active fault in any of the converter legs. Firstly, the corresponding phase leg with an active fault is being shut down to avoid any damage caused by the fault. In the case of active faults in multiple phases, all the affected phase legs are switched off. Thereafter, for the remaining in operation phases with healthy states, the PWM carrier phase shifts are re-distributed between each other with equal phase shifts.

To ensure the converter operation with reduced number of phases, the fault-tolerant operation algorithm is integrated into the overall converter control algorithm, as shown in Fig. 3.4 by means of the corresponding flowchart. The overall converter control algorithm consists of three paths – main path, control path, and fault-tolerant path. The main path is initiated in any case by generating PWM outputs, sampling indirect DC link current, phase current reconstruction, and fault condition monitoring. If no reset or shutdown is requested and there is no active fault, the control path is proceeded sequentially. The control path consists of the duty cycle corrections by the inner current balancing controller and the main duty cycle calculation by the outer voltage control loop with returning to the main path. If a new active fault state is detected by the end of the main path, the fault-tolerant path is proceeded. The fault-tolerant path follows the faulty phase shutdown, PWM carrier re-distribution enabling the state of fault-tolerant algorithm (setting to "true"). If the reset or shutdown is requested, the main program returns to the end, but at the start, the control mode is being reset to the normal mode with all phases being activated. Hence, the fault condition is cleared by each reset, and the algorithm will need to make one full cycle (equivalent to one switching period) to switch back to the fault-tolerant mode if any active fault persists.
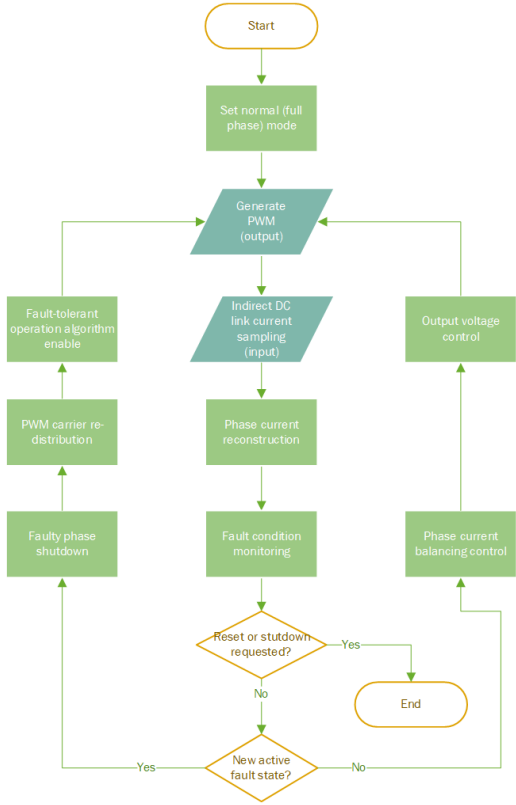
Fig. 3.4. Flowchart of the overall converter control with integrated fault-tolerant operation algorithm.

For the experimental verification of the fault-tolerant operation algorithm, the fault conditions are modelled intentionally. A switch open circuit event is generated by shortening the corresponding gate driver input. Inductor fault is generated by a separate switch, causing an open circuit fault in phase 5. The converter control algorithm is equipped with an additional external input signal for switching on or off the fault tolerant algorithm part. Hence, the converter can be operated in different modes – in normal (healthy state) with all five active phases, with an active fault in one or multiple phases without transition to fault-tolerant algorithm or with automatic transition to fault-tolerant algorithm. The comparison between different steady state operation modes under high load is shown in Fig. 3.5. Although all converter phases were in operation, only phase 1, 4, and 5 currents are shown for the sake of simplicity and better overview. The experimental results show that at steady state the fault-tolerant operation algorithm minimizes the negative effects of an active open-circuit fault, and the converter can perform its functions with optimal performance. Under high load conditions the phase currents show high peaks, caused by inductor partial saturation due to an active fault. The transition to fault-tolerant operation reduces the current peak and, hence, the inductor saturation effects significantly, thus, allowing operation with much better performance.

Fig. 3.5. The compassion between different mode steady state operation

The measured voltages and currents at converter input and output ports is shown in Fig. 3.6. In a normal 5-phase operation with a duty cycle of 25 %, the currents show higher ripples in comparison with the 4-phase operation, where ripples are compensated by inductor coupling. This is caused by relatively large influence of switching frequency 5th harmonic on the total current in normal operation. In the case of a fault-tolerant operation in a 4-phase mode, the switching frequency 4th harmonic influence on total current is reduced due to a more favourable PWM carrier phase shift re-configuration. Nevertheless, the switching frequency component is present due to different pulse delays through the drivers and imbalances in the core that can be further optimized by, e.g., implementing the active phase-shift control described in [52].

Consequently, due to the increased coupled inductor hysteresis (iron) losses, the converter efficiency decrease is observed in case of operation with active fault. Due to transition to fault-tolerant operation, the efficiency decrease is being reduced or even eliminated.

a) normal operation   b) operation with single phase fault   c) fault-tolerant operation
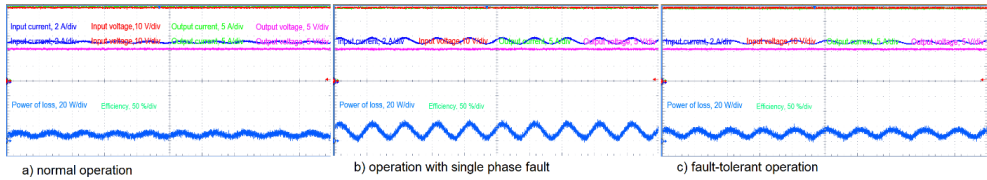
Fig. 3.6. The comparison between measured voltages and currents at converter input and output ports in different steady state operation modes.

The converter steady state operation has been verified in full duty cycle range. The comparison between the current rms and ripple value measurements are presented for normal operation, operation with single phase fault, and fault-tolerant operation. Phase current and total current rms values are shown for three different modes in Fig. 3.7. Phase current maximum ripple and total current ripple values are shown for three different modes in Fig. 3.8.
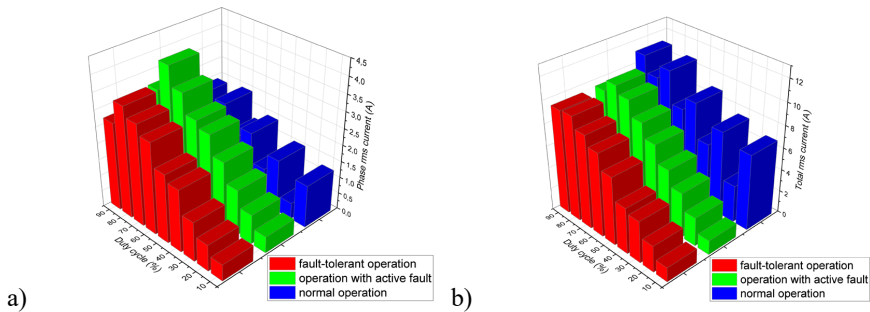
Fig. 3.7. Comparison between a) phase current and b) total output current rms values in different operation modes.
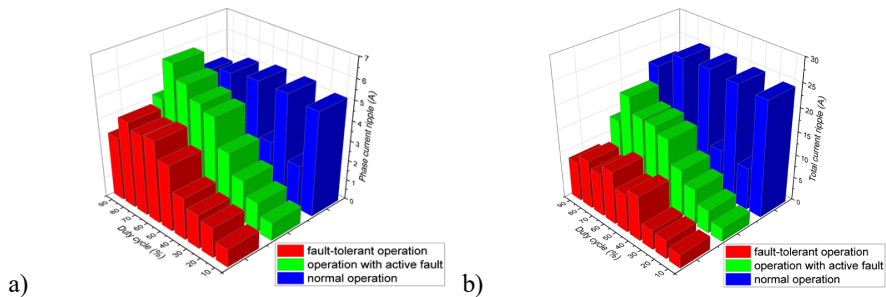
Fig. 3.8. Comparison between a) phase current and b) total output current ripples in different operation modes.

The current ripples in normal 5-phase operation mode reach maximums at duty cycle values of 10 %, 30 %, 50 %, 70 %, and 90 %, but the minimums are observed at duty cycle values of 20 %, 40 %, 60 %, and 80 %, as expected in a 5-phase converter with coupled inductors. The maximum and minimum current ripple values in normal operation mode have impact on the corresponding rms values. Therefore, the phase and total current rms values represent the changes in ripples with a rising tendency when the duty cycle is increasing.

In case of operation with active fault, the current ripples and rms values are rising by increasing the duty cycle. The same tendency is observed in the 4-phase fault-tolerant operation mode, however, the phase and total current rms values are lower in comparison with an operation with active fault. The maximum phase current ripples and the total current ripple show a significant decrease by enabling the fault-tolerant operation algorithm in case of an active fault, especially in case of total current ripples. Hence, the proposed algorithm helps to reduce ripples and, sequentially, the current rms values, thus, improving efficiency in wide duty cycle range.

Finally, the converter dynamic behaviour is analysed by evaluating the transitions between different modes of converter operation at nominal duty cycle. The phase currents during transition between three different modes of operation are shown in Fig. 3.9 under the circumstances of intentionally applied 2.5 ms delay for the fault-tolerance algorithm turn-on. The phase currents during an automatic transition to fault-tolerant operation right after the fault occurrence are shown for high and moderate load in (Fig. 3.10).
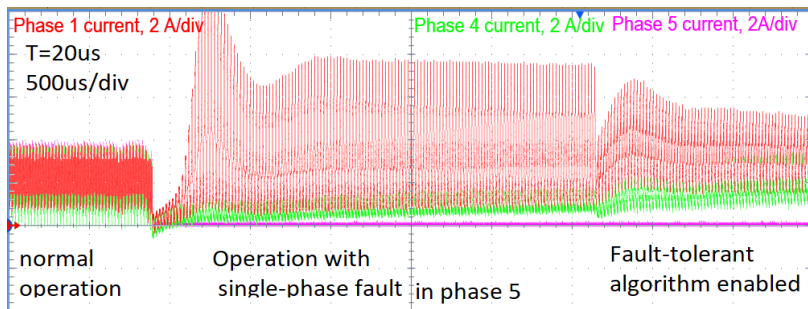
Fig. 3.9. Phase currents during the transition between normal operation, operation with single-phase fault, and fault-tolerant operation with additional delay.
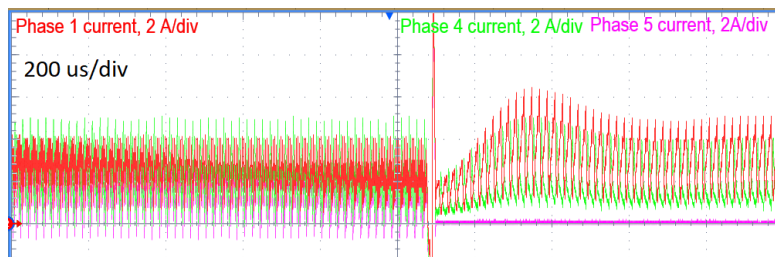
Fig. 3.10. The phase currents during an automatic transition to fault-tolerant operation right after the fault occurrence under high load conditions.

The transitions between different modes can be realized very fast. Right after the fault occurrence, an algorithm requires one or two switching periods to re-distribute the PWM carrier phase shifts and set-up the fault-tolerant operation mode. Practically, the transition lasts 20–40 μs, including fault detection and identification, but the acquired transition time slot is small enough to avoid any risks of converter damage. Hence, further converter operation with minor performance degradation is possible even with an active fault. However, care must be taken during the output capacitance value estimation because the output capacitor must ensure voltage stability during transients. A more detailed analysis is shown in [46].

3.3. Conclusions

The DC link current waveforms reflect the most common converter failure modes, and the proposed ICM based technique can detect the overall fault condition and specify the failed component within 10–20 us in the case of open circuit and in less than 4 us in the case of short circuit even in a converter with strongly magnetically coupled inductors. The fault state detection and identification method show reliable performance within the whole converter duty cycle range, including the transient operation and protection against pseudo-fault detection events.

The designed fault-tolerant control system can avoid converter shutdown and provide an effective solution for converter operation with optimal performance in case of active semiconductor switch or inductor open circuit fault. The proposed algorithm has shown smaller current ripples and rms values, loss power reduction, and efficiency improvements by up to 2 % in comparison with the operation with active fault without fault-tolerant algorithm applied. In comparison with a normal operation, the application of fault-tolerant operation algorithm results in minor efficiency decrease and ensures high performance especially under high load conditions. A fast transition to fault-tolerant algorithm is performed in case of fault occurrence and further converter operation with minor performance degradation.

4. ENERGY EFFICIENCY IN AUXILIARY CONVERTERS

Auxiliary converter system efficiency is the major key to achieve the objective of energetically and economically effective technology. The auxiliary systems must be provided with a reliable power supply that consumes minimum amount of energy for the specified purposes. This chapter discusses the potential of wide bandgap semiconductor use in auxiliary converters and analyses the further energy saving measures. A detailed analysis is shown in [2].

4.1.   Wide bandgap semiconductor utilization in auxiliary converters

Wide bandgap (WBG) semiconductor devices have gained an increased interest within the last few decades in different fields and applications. While the WBG materials like Ge, GaAs, InP, ZnO, and ZnS are less commonly used in power electronics, the silicon carbide (SiC) and gallium nitride (GaN) semiconductors are the most frequently mentioned and applied types of WBG devices that are currently spreading on the market [59]. In comparison with the classical silicon (Si), the SiC and GaN WBG semiconductors offer significantly lower switching losses and operation capabilities at considerably higher switching frequencies [59]–[65], resulting in choice of smaller passive filter components [63], better EMI performance, and elimination of acoustic effects [60]. Furthermore, their ohmic conduction characteristics lead to reduced conduction losses at light loads [55], but combined with switching loss minimization, WBG semiconductors offer a potential for achieving very high efficiencies in typical power electronics applications [62]–[66].

SiC MOSFET devices have multiple considerable advantages in comparison with Si IGBTs. SiC shows higher breakdown electric field, wide energy bandgap of 3.23 eV, higher saturation velocity, thermal conductivity and melting point [59], thus, ensuring higher blocking voltage, switching frequency and withstanding thermal stresses with reduced heat sink volume. As the result, the operational parameters of SiC semiconductors show significantly higher performance compared to Si [61]–[64], [66] but slightly poorer results than GaN [61]–[63]. While the SiC MOSFETs are becoming to be widely implemented in different fields with higher voltage levels, the GaN devices are less common and still intended for use in specific low voltage power converters [67], [68]. Despite that, GaN semiconductors nowadays have very tiny market share, still not available in voltage classes above 650 V, have lower reliability [59], [61] and, therefore, are challenging to be utilized in typical applications without transition to multilevel topologies [61], [66]. Hence, in comparison with GaN the price and availability on the market of SiC semiconductor devices is more competitive and is expected to approach the Si level in the next five years [59]. GaN semiconductors are expected to show the highest market share growth [59] by reducing the price and improving reliability. Hence, the SiC MOSFETs offer an attractive solution for power electronics converter design in typical inverter applications [60], [61] already nowadays, allowing to achieve high performance.

Application of WBG semiconductor devices in power electronics applications leads to considerable loss reduction and efficiency improvements. In [63], the Si IGBTs, SiC MOSFETs and GaN HEMTs have been evaluated in a T-type single-phase inverter and shown

enhancements in switching performance, efficiency rise, heat sink and output filter volume reduction with lower harmonic distortions by moving from Si to GaN semiconductor implementation, respectively. Considerable efficiency rise has been achieved by Si/SiC hybrid switch utilization in a 3-level NPC inverter in [60]. In [65], the GaN potential of very high-power density is shown in different battery charging applications from 5 V 240 W up to 11 kW and 1 kV. While [67] and [23] have experimentally verified the GaN fast switching performance in low voltage applications, in [68], it is approved that a GaN-based inverter can be designed for operation under harsh cryogenic conditions despite the reliability issues mentioned in [59]. Furthermore, studies [69]–[71] have verified that application of SiC MOSFETs in auxiliary converters in different types of railway application gives not only considerable loss reduction, but also leads to more compact design and reduced weight due to less powerful cooling system and, hence, reduces the overall vehicle energy consumption. In [69], it has been shown that the SiC MOSFET use allows the lightweight converter design by reducing losses and heat sink volume; however, a more careful busbar design is required to eliminate parasitic effects and achieve optimal switching performance. In [70], the SiC devices ensure efficiency increase with reduced LC filter element volume reduction due to faster switching, resulting in higher auxiliary converter power density. The loss reduction correlated to SiC use has been shown also in [71], but even more considerable efficiency improvement was observed in combination with more advanced DC/DC converter design with optimized commutation loop [71]. Hence, implementation of WBG devices becomes especially advantageous in combination with the optimized auxiliary converter design.

The performance of SiC and GaN semiconductors in a 3-phase 3-level inverter is evaluated and compared. The acquired line voltage and phase current waveforms with the output current frequency of 50 Hz and variable switching frequency of 1 kHz, 10 kHz, and 100 kHz, for inverter operation with SiC MOSFETs and GaN FETs is shown in Fig. 4.1. The corresponding thermal images of loss power distribution with the output current frequency of 50 Hz and variable switching frequency of 1 kHz, 10 kHz, and 100 kHz for inverter operation with SiC MOSFETs and GaN FETs is shown in Fig. 4.2. Inverter operation with both compared types of WBG semiconductor devices shows similar voltage and current waveforms. As the driver parameters have been adjusted for similar switching performance in terms of turn-on and off times and voltage ringing effects, the resultant line voltage and phase current waveforms are identical in both cases. With the increase in switching frequency, a significant reduction in current ripples is observed and in the case of switching frequency of 100 kHz the current ripples are almost eliminated, resulting in lower THD and conduction losses. However, at higher switching frequency, the inverter efficiency decreases.

Inverter input and output power measurements have been performed in wide range of AC frequency and switching frequency for efficiency and loss power estimation. The inverter efficiency and loss power depending on the switching frequency is shown for an operation with SiC and GaN semiconductors with AC frequency of 50 Hz in Fig. 4.3. The inverter efficiency and loss power depending on the AC frequency at 10 kHz switching frequency is shown in Fig. 4.4. The efficiency depending on the inverter switching frequency shows the maxima at approximately 10 kHz, where the balance between the switching losses and current ripples is

achieved in the case of operation with SiC MOSFETs. When operated with GaN FETs, the inverter shows higher efficiency even at low frequencies, resulted from more efficient conduction in freewheeling operation. In contrast with SiC MOSFETs, where the Schottky diode has a forward voltage drop, the GaN FETs have pure resistive conduction losses if the gate-source voltage is set to high. Hence, the GaN FETs show more efficient conduction that has a more considerable impact at light loads and low switching frequencies, where the conduction losses are dominant. With higher switching frequencies the switching losses become dominant, and that reduces the efficiency. The efficiency depending on the inverter output AC frequency shows the values between 98 % and 99 % in wide range of operation with GaN FETs. In the case of SiC MOSFETs, the inverter efficiency is lower by 1…1.5 %.
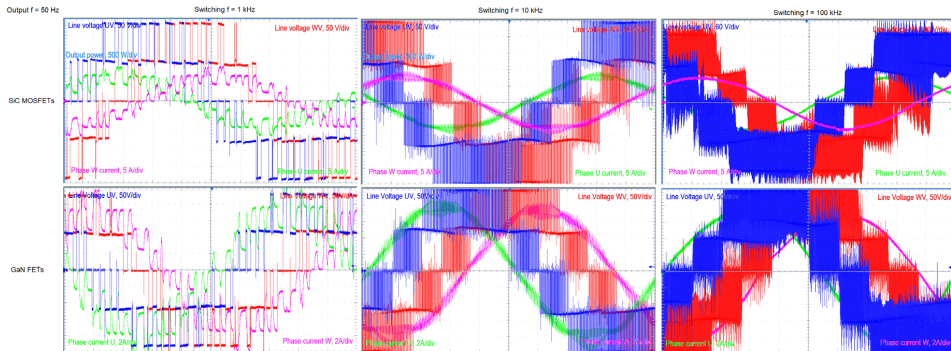
Fig. 4.1. Line voltage and phase current waveforms with the output current frequency of 50 Hz and variable switching frequency of 1 kHz, 10 kHz, and 100 kHz for inverter operation with SiC MOSFETs and GaN FETs.
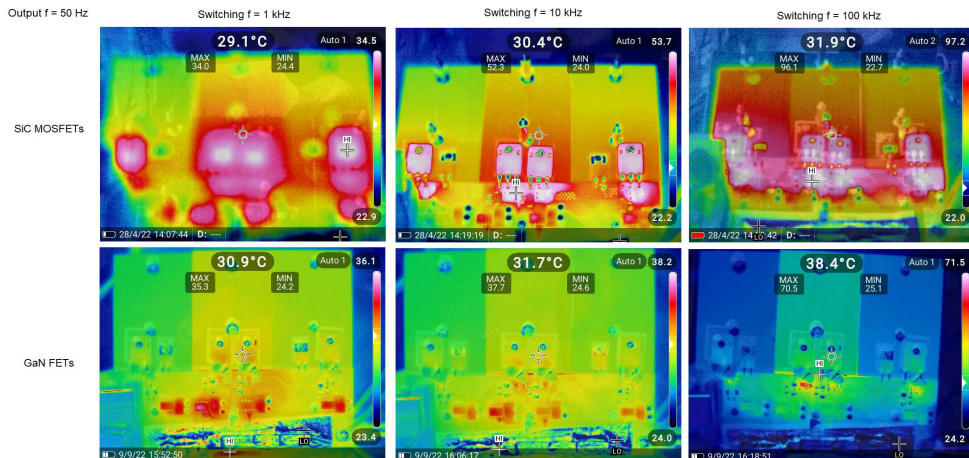
Fig. 4.2. Thermal images of loss power distribution with the output current frequency of 50 Hz and variable switching frequency of 1 kHz, 10 kHz, and 100 kHz for inverter operation with SiC MOSFETs and GaN FETs.
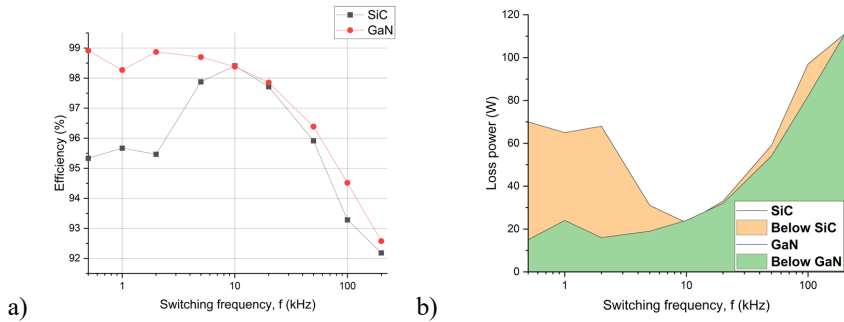
Fig. 4.3. Comparison between inverter a) efficiency and b) loss power depending on the switching frequency for operation with the SiC and GaN semiconductors.
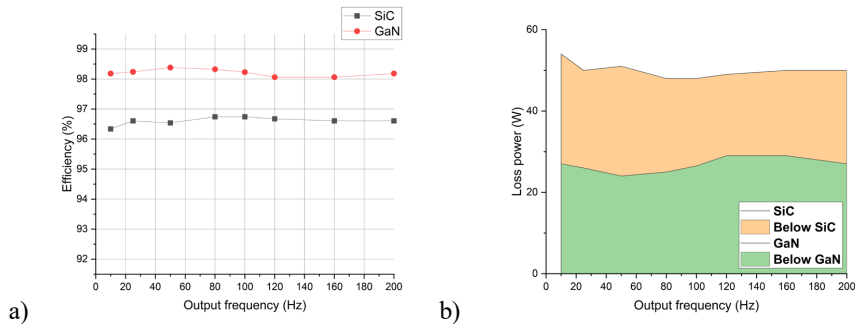
Fig. 4.4. Comparison between inverter a) efficiency and b) loss power depending on the AC frequency for operation with the SiC and GaN semiconductors.

The loss distribution analysis shows considerable heat dissipation in snubber circuits, especially at high switching frequencies. Comparison of SiC and GaN operations in terms of heat dissipation from semiconductor devices is obviously showing the benefits of GaN FET operation, where the temperature of transistors is lower. Hence, the WBG semiconductor comparison results approve that GaN has lower total losses and can achieve higher efficiencies.

Finally, the single semiconductor switch costs, total semiconductor costs and other component costs (i.e., PCB, passive components, integrated circuits, controller board, etc.) are estimated for comparison between the Si, SiC, and GaN semiconductors and depicted in Fig. 4.5. The initial purchase price of WBG semiconductor devices is very high. In comparison with GaN and SiC, the initial price of a similar Si IGBT is 71 % and 59 % lower, respectively. However, in terms of the total system component price, the Si semiconductors are only 8 % and 5 % cheaper, than the GaN and SiC ones, respectively, but the difference in terms of an overall system would be insignificant. Although the economic influence of considerable loss reduction and efficiency increase within an auxiliary converter life cycle is challenging to determine, it can be assumed, that the total life cycle costs are very likely to be reduced by utilizing the WBG devices. Nevertheless, as discussed in [47], the GaN FETs still have reliability issues resulting

in higher failure rate that can lead to additional unforeseen maintenance costs in field operation. Therefore, in terms of economic aspects the SiC MOSFETs are more likely to be recommended for auxiliary converters in transportation applications nowadays.
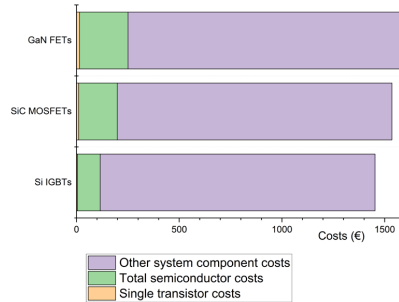
Fig. 4.5. Comparison between the Si, SiC, and GaN single semiconductor switch costs, total semiconductor costs, and other component costs.

4.2. Variable frequency auxiliary drive

Auxiliary power demand in all types of vehicles has been gradually increasing within the last decades, caused by more safety and comfort systems being introduced, as well as the electrification of auxiliary systems. As shown in [72], the operation of auxiliary systems has considerable impact on the overall vehicle energy consumption. The largest part of auxiliary power in vehicles make drive systems for heating, ventilation and air conditioning (HVAC), power steering unit (PSU) and air compressor, having power ratings ranging from 1 kW [72] up to 190 kVA [69]. Despite the significant technology advancements in power electronics and electrical drives, most of auxiliary systems in modern vehicles use a conservative design approach with a single auxiliary converter system producing 50 Hz AC supply for all systems simultaneously and an induction machine (IM) – a contactor system for each system drive [73]. Consequentially, the auxiliary drives are operating in cyclic load conditions with regular IM starting under load, nominal point operation and rest phases, resulting in high thermal and mechanical stresses and low efficiency of the system. Hence, a variable frequency drive concept operating with constant load can reduce the stresses and save energy. Moreover, the application of multi-level inverter topology to auxiliary drive can enhance the efficiency of the system [74]. Therefore, it is reasonable to investigate a novel auxiliary drive concept for application in electric transportation that ensures optimal efficiency and reliability for long life operation.

A case study on different auxiliary drive solutions is carried out on a vehicular air compressor example for a comparative result assessment. A permanent magnet synchronous machine (PMSM) is considered for the comparison with IM that is operated in nominal point with direct start versus variable frequency operation. In addition, an industrial frequency converter operation is compared with the supply from the GaN-based 3-level NPC inverter. The initial data about the air compressor system and electrical drive parameters is obtained

experimentally to build up the simulation model that is used for the case study comparative analysis. The compressed air consumption is modelled by a simplified mission profile repeating the city bus operation patterns in Jelgava, Latvia [75].

The induction machine torque and speed patterns for the system turn-on and further steady state operation in case of cyclic load and variable frequency operation are shown in Fig. 4.6 a) and b), respectively. The comparison between the pneumatic system air pressure patterns for cyclic and variable frequency operation are shown in Fig. 4.7 a) and b), respectively. The comparison between the system turn-on energy consumptions and steady state power are shown in Fig. 4.8 a) and b), respectively. The auxiliary drive for air compressor in a variable frequency operation mode shows stable system pressure, gradual transitions between turn-on and steady state, energy consumption reduction by 2 % at turn-on and by 2.5 % at steady state. Further energy savings are achieved by utilizing PMSM instead of IM, as it achieves better efficiency at partial load below the base speed, as well as by implementing GaN FETs in a 3-level NPC inverter topology that show efficiency about 99 % even at partial load [2]. Thus, by operating the system constantly with partial load, the thermal and mechanical stresses are minimized by reducing the component wear out due to frequent heavy starts. Hence, a variable frequency drive concept can reduce the stresses and save energy of the system.

The proposed auxiliary drive concept ensures the highest efficiency in operation with partial load, light and balanced loading without heavy starts, significantly reduced wear out of components, and energy savings by about 2.5 %. By utilizing the PMSM drive with GaN FET NPC inverter, the total efficiency improvement is estimated to reach about 10 %. Moreover, by operating the system in variable frequency mode, the thermal and mechanical stresses are minimized. As a result, the auxiliary drive system can be designed with downsized components, at the same time achieving a more reliable field operation with an increased lifetime.
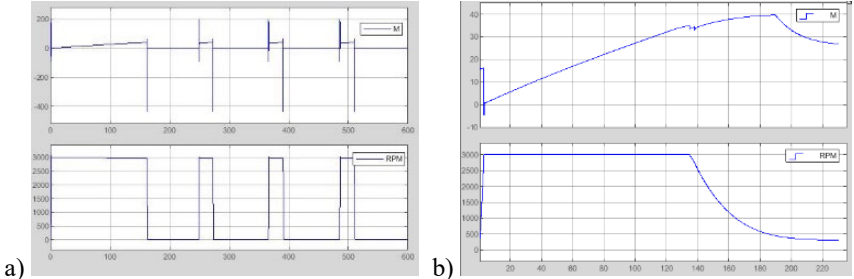
Fig. 4.6. The induction machine torque and speed patterns for modes: a) cyclic, b) variable frequency.
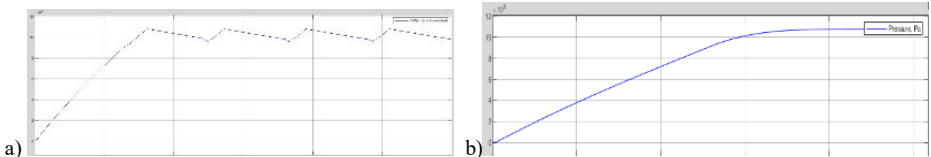
Fig. 4.7. The pneumatic system air pressure patterns for modes: a) cyclic, b) variable frequency.
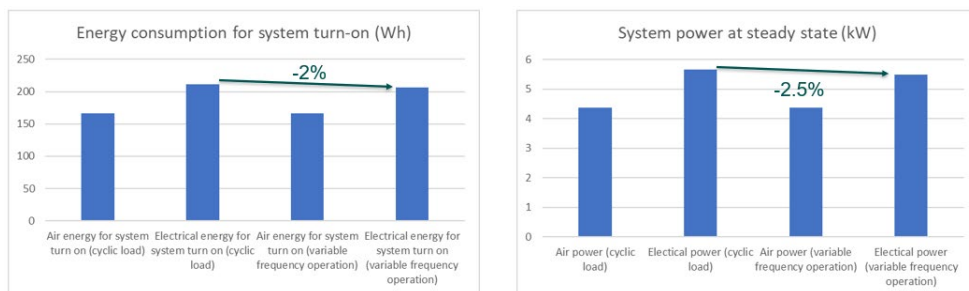
Fig. 4.8. The comparison between operation modes: a) energy consumption at turn-on, b) average power.

4.3. Conclusions

Auxiliary converter systems in transportation applications require novel solutions and designs to meet the rising auxiliary power demands. The proposed auxiliary inverter operation in variable frequency drive system shows high efficiency in wide range, therefore it has large potential for energy savings in a vehicular auxiliary system, i.e., air compressor, steering power unit, and air conditioning system. The 3-level inverter topology allows utilization of semiconductors with lower breakdown voltage, minimizes the current ripples, THD and EMI, as well as offers more efficient operation with reduced switching losses. In combination with the WBG semiconductor use, the proposed 3-level inverter in variable frequency operation has even more benefits in terms of loss minimization in full operational range of auxiliary drives, especially by enabling considerably more efficient operation at light loads and at reduced voltage.

The wide bandgap semiconductors have shown excellent performance with efficiencies above 96 % in typical auxiliary converter operation modes. Utilization of GaN semiconductors in a 3-phase 3-level inverter for auxiliary variable frequency drive application results in the maximum efficiency in all operating modes; however, it has the highest initial purchase costs and possibility of failure leading to risks of higher total life cycle costs due to possibility of additional maintenance in field operation. In comparison with Si, a high initial price for SiC devices is likely to be compensated by the considerable loss reduction and reliable field operation. Therefore, the use of auxiliary converters utilizing SiC semiconductors in transportation applications is currently more advisable, as the inverter design with SiC MOSFETs and Schottky diodes is nowadays still technically and economically more effective.

The proposed auxiliary drive concept in combination with the PMSM drive with GaN FET NPC inverter shows the highest efficiency in operation with partial load, light and balanced loading without heavy starts, significantly reduced wear out of components, thermal stress reduction by 80 %, and energy savings by about 10 %. By operating the system in variable frequency mode, the thermal and mechanical stresses are minimized, resulting in downsized components, at the same time achieving more reliable field operation with an increased lifetime.

CONCLUSIONS

Electric vehicles require volume- and cost-effective, efficient and modular auxiliary converter system design. By introducing a set of technological advancements discussed in the Thesis, the aim of designing an energetically and economically effective technology for auxiliary converter systems in electric vehicles can be fulfilled. The total energy savings by auxiliaries can reach up to 10 %, with stress reduction by up to 80 % and considerable functionality improvements in reliability and fault tolerance.

The novel indirect current measurement (ICM) technique allows to achieve a cost-efficient auxiliary converter sensing and measurement design with functionality of the current sensing and balancing, fault detection and identification, as well as the fault-tolerant operation.

The ICM implementation in a multi-phase DC converter has shown adequate accuracy for current balancing with measurement errors below 0.5 A, resulting in no efficiency degradation, fast fault detection and identification capability within one converter switching period or 20 μs and efficient fault-tolerant operation that can allow a converter operation with active fault condition and improve efficiency by up to 2 %. The proposed ICM technique implementation in combination with intelligent control system is considered as a key technology for the converter high efficiency, optimized performance, fault tolerance and reliable power supply for safety critical systems.

Wide bandgap semiconductor utilization in combination with ICM results in significantly higher efficiency and reduced volume that allows to achieve higher auxiliary converter power density level, faster operation, and power loss reduction by up to 5 %. Moreover, the application of the wide bandgap devices is technically and economically effective.

Use of variable frequency drive concept in vehicular auxiliary systems with a wide bandgap device-based multi-level inverter has shown low total harmonic distortion and electromagnetic interference levels with high efficiency in wide operation range that results in energy savings of approximately 10 %, longer lifetime, and more reliable operation with thermal stresses being reduced by 80 %.

Within the scope of the future research, the ICM concept can be extended for other multi-phase and multi-level auxiliary converter topologies, utilizing wide bandgap semiconductors to propose a solution for the complete auxiliary system modernization. The achieved results have a strong potential for commercialization and can be further developed for testing in the application relevant environment, certification, type approval and release to the market within the next four years.

REFERENCES

[1]   P. Hołyszko, D. Zieliński, A. Niewczas, J. Rymarz, and E. Dębicka, "Ensuring the Continuity of Power Supply to the On-Board Auxiliary Devices of the Trolleybus through the Recuperation of Kinetic Energy," *Energies*, vol. 14, no. 16, p. 5035, Aug. 2021, doi: 10.3390/en14165035.

[2]   A. Bogdanovs, O. Krievs, and J. Pforr, "Wide Bandgap SiC and GaN Semiconductor Performance Evaluation in a 3-Phase 3-Level NPC Inverter for Transportation Application," *2022 IEEE 63th International Scientific Conference on Power and Electrical Engineering of Riga Technical University (RTUCON)*, Riga, Latvia, 2022, pp. 1–7, doi: 10.1109/RTUCON56726.2022.9978767.

[3]   L. Kondratieva, A. Bogdanovs, L. Overianova, I. Riabov, S. Goolak, "Determination of the Working Energy Capacity of the On-Board Energy Storage System of an Electric Locomotive for Quarry Railway Transport during Working with a Limitation of Consumed Power," *Archives of Transport*, vol. 65, no. 1, pp. 119–136, doi:10.5604/01.3001.0016.2631

[4]   S. He et al., "Digital Collaborative Development of a High Reliable Auxiliary Electric Drive System for eTransportation: From Dual Three-Phase PMSM to Control Algorithm." In: *IEEE Access*, vol. 8, pp. 178755–178769, 2020, doi: 10.1109/ACCESS.2020.3027633.

[5]   T. M. Jahns and B. Sarlioglu, "The Incredible Shrinking Motor Drive: Accelerating the Transition to Integrated Motor Drives." In: *IEEE Power Electronics Magazine*, vol. 7, no. 3, pp. 18–27, Sept. 2020, doi: 10.1109/MPEL.2020.3011275.

[6]   D. Cittanti, E. Vico, E. Armando, and R. Bojoi, "Analysis and Conceptualization of a 400V 100 kVA Full-GaN Double Bridge Inverter for Next-Generation Electric Vehicle Drives," *2022 IEEE Transportation Electrification Conference & Expo (ITEC)*, Anaheim, CA, USA, 2022, pp. 740–747, doi: 10.1109/ITEC53557.2022.9813847.

[7]   S. Utz and J. Pforr, "Turn-on behavior of automotive multi-phase converters with coupled inductors," *2012 15th International Power Electronics and Motion Control Conference (EPE/PEMC)*, Novi Sad, Serbia, 2012, pp. LS3c.3-1-LS3c.3–8, doi: 10.1109/EPEPEMC.2012.6397434.

[8]   S. Utz and J. Pforr, "Impact of input and output voltage perturbation on the behavior of automotive multi-phase converters with coupled inductors," *2011 IEEE Energy Conversion Congress and Exposition*, Phoenix, AZ, USA, 2011, pp. 4169–4176, doi: 10.1109/ECCE.2011.6064337.

[9]   J. Czogalla, Jieli Li, and C. R. Sullivan, "Automotive application of multi-phase coupled-inductor DC-DC converter," *38th IAS Annual Meeting on Conference Record of the Industry Applications Conference*, 2003., Salt Lake City, UT, USA, 2003, pp. 1524–1529 vol.3, doi: 10.1109/IAS.2003.1257758.

[10]   S. Utz and J. Pforr, "Current-balancing controller requirements of automotive multi-phase converters with coupled inductors," *2012 IEEE Energy Conversion Congress and*

Exposition (ECCE), Raleigh, NC, USA, 2012, pp. 372–379, doi: 10.1109/ECCE.2012.6342798.

[11]   H. Kim, M. Falahi, T. M. Jahns, and M. W. Degner, "Inductor Current Measurement and Regulation Using a Single DC Link Current Sensor for Interleaved DC–DC Converters," in *IEEE Transactions on Power Electronics*, vol. 26, no. 5, pp. 1503–1510, May 2011, doi: 10.1109/TPEL.2010.2084108.

[12]   J. C. Schroeder, M. Petersen, and F. W. Fuchs, "One-sensor current sharing in multiphase interleaved DC/DC converters with coupled inductors," *2012 15th International Power Electronics and Motion Control Conference (EPE/PEMC)*, Novi Sad, Serbia, 2012, pp. DS3c.1-1-DS3c.1–7, doi: 10.1109/EPEPEMC.2012.6397338.

[13]   Y. -H. Cho, A. Koran, H. Miwa, B. York, and J. -S. Lai, "An active current reconstruction and balancing strategy with DC-link current sensing for a multi-phase coupled-inductor converter," *2010 IEEE Energy Conversion Congress and Exposition*, Atlanta, GA, USA, 2010, pp. 3414–3419, doi: 10.1109/ECCE.2010.5618316.

[14]   S. Mariethoz, A. G. Beccuti, and M. Morari, "Model predictive control of multiphase interleaved DC-DC converters with sensorless current limitation and power balance," *2008 IEEE Power Electronics Specialists Conference*, Rhodes, Greece, 2008, pp. 1069–1074, doi: 10.1109/PESC.2008.4592071.

[15]   J. Gordillo and C. Aguilar, "A Simple Sensorless Current Sharing Technique for Multiphase DC–DC Buck Converters," in *IEEE Transactions on Power Electronics*, vol. 32, no. 5, pp. 3480–3489, May 2017, doi: 10.1109/TPEL.2016.2592240.

[16]   K. -Y. Hu, Y. -S. Chen, and C. -H. Tsai, "A Digital Multiphase Converter with Sensor-less Current and Thermal Balance Mechanism," *2018 IEEE Asian Solid-State Circuits Conference (A-SSCC)*, Tainan, Taiwan, 2018, pp. 175–178, doi: 10.1109/ASSCC.2018.8579301.

[17]   J. Han and J. -H. Song, "Phase Current-Balance Control Using DC-Link Current Sensor for Multiphase Converters with Discontinuous Current Mode Considered." In: *IEEE Transactions on Industrial Electronics*, vol. 63, no. 7, pp. 4020–4030, July 2016, doi: 10.1109/TIE.2016.2530781.

[18]   H. -C. Chen, C. -Y. Lu, and C. -H. Lu, "Control of Bidirectional Interleaved DC-DC Converter with Single Current Sensor," *2018 IEEE Energy Conversion Congress and Exposition (ECCE)*, Portland, OR, USA, 2018, pp. 2171–2177, doi: 10.1109/ECCE.2018.8557828.

[19]   H. -C. Chen, C. -Y. Lu, and L. -M. Huang, "Decoupled Current-Balancing Control with Single-Sensor Sampling-Current Strategy for Two-Phase Interleaved Boost-Type Converters." In: *IEEE Transactions on Industrial Electronics*, vol. 63, no. 3, pp. 1507–1518, March 2016, doi: 10.1109/TIE.2015.2498135.

[20]   R. P. Singh and A. M. Khambadkone, "Current Sharing and Sensing in N-Paralleled Converters Using Single Current Sensor." In: *IEEE Transactions on Industry Applications*, vol. 46, no. 3, pp. 1212–1219, May-june 2010, doi: 10.1109/TIA.2010.2045333.

[21]   M. Stadler and J. Pforr, "Multi-phase Converter for Wide Range of Input Voltages with Integrated Filter Inductor," *2006 12th International Power Electronics and Motion Control Conference*, Portoroz, Slovenia, 2006, pp. 106–111, doi: 10.1109/EPEPEMC.2006.4778384.

[22]   V. Yousefzadeh and S. Choudhury, "Nonlinear digital PID controller for DC-DC converters," *2008 Twenty-Third Annual IEEE Applied Power Electronics Conference and Exposition*, Austin, TX, USA, 2008, pp. 1704–1709, doi: 10.1109/APEC.2008.4522956.

[23]   K. Kroics, "Design of Interleaved GaN Transistor Based Buck Converter with Directly Coupled Foil Winding Inductor," CIPS 2020; *11th International Conference on Integrated Power Electronics Systems*, Berlin, Germany, 2020, pp. 1–6.

[24]   K. Kroics, J. Zakis, and U. Sirmelis, "Multiphase interleaved DC-DC converter with directly and inversely coupled inductors," *2016 57th International Scientific Conference on Power and Electrical Engineering of Riga Technical University (RTUCON)*, Riga, Latvia, 2016, pp. 1–6, doi: 10.1109/RTUCON.2016.7763102.

[25]   A. Bogdanovs, O. Krievs, and J. Pforr, "Indirect DC link current measurement technique using an op-amp circuit in an automotive DC converter with coupled inductors," *PCIM Europe digital days 2020; International Exhibition and Conference for Power Electronics, Intelligent Motion, Renewable Energy and Energy Management*, Germany, 2020, pp. 1–8.

[26]   S. Kim, J. -I. Ha, and S. -K. Sul, "Single shunt current sensing technique in three-level PWM inverter," *8th International Conference on Power Electronics – ECCE Asia*, Jeju, Korea (South), 2011, pp. 1445–1451, doi: 10.1109/ICPE.2011.5944454.

[27]   H. Shin and J. -I. Ha, "Phase Current Reconstructions from DC-Link Currents in Three-Phase Three-Level PWM Inverters," in *IEEE Transactions on Power Electronics*, vol. 29, no. 2, pp. 582–593, Feb. 2014, doi: 10.1109/TPEL.2013.2257866.

[28]   X. Li, S. Dusmez, B. Akin, and K. Rajashekara, "A new SVPWM for phase currents reconstruction of three-phase three-level T-type converters," *2015 IEEE Applied Power Electronics Conference and Exposition (APEC)*, Charlotte, NC, USA, 2015, pp. 1582–1588, doi: 10.1109/APEC.2015.7104558.

[29]   X. Li, S. Dusmez, B. Akin, and K. Rajashekara, "A New SVPWM for the Phase Current Reconstruction of Three-Phase Three-level T-type Converters," in *IEEE Transactions on Power Electronics*, vol. 31, no. 3, pp. 2627–2637, March 2016, doi: 10.1109/TPEL.2015.2440421.

[30]   Y. Son and J. Kim, "A Novel Phase Current Reconstruction Method for a Three-Level Neutral Point Clamped Inverter (NPCI) with a Neutral Shunt Resistor," *Energies*, vol. 11, no. 10, p. 2616, Oct. 2018, doi: 10.3390/en11102616.

[31]   J. -J. You, J. -H. Jung, C. -H. Park, and J. -M. Kim, "Phase current reconstruction of three-level Neutral-Point-Clamped(NPC) inverter with a neutral shunt resistor," *2017 IEEE Applied Power Electronics Conference and Exposition (APEC)*, Tampa, FL, USA, 2017, pp. 2598–2604, doi: 10.1109/APEC.2017.7931064.

[32]   A. Suzdalenko, J. Zakis, and O. Krievs, "Single-loop Current Sensorless Control with Self-detection of Conduction Losses Applied to Neutral Point Clamped Multilevel Converter," *2019 11th International Conference on Electrical and Electronics Engineering (ELECO)*, Bursa, Turkey, 2019, pp. 250–254, doi: 10.23919/ELECO47770.2019.8990464.

[33]   F. Blaabjerg, J. K. Pedersen, U. Jaeger, and P. Thoegersen, "Single current sensor technique in the DC link of three-phase PWM-VS inverters: a review and a novel solution." In: *IEEE Transactions on Industry Applications*, vol. 33, no. 5, pp. 1241–1253, Sept.-Oct. 1997, doi: 10.1109/28.633802.

[34]   T. C. Green, B. W. Williams, B.W, "Derivation of motor line-current waveforms from the DC-link current of an inverter", *IEE Proceedings B (Electric Power Applications)*, 1989, 136, (4), pp. 196–204, DOI: 10.1049/ip-b.1989.0026.

[35]   Lu Haifeng, Sheng Shuang, Guo Ruijie, Qu Wenlong, and Wu Lixun, "Phase current sensor fault-tolerant technique using information of DC side current in two-level inverter," *2013 International Conference on Electrical Machines and Systems (ICEMS)*, Busan, 2013, pp. 1648–1651, doi: 10.1109/ICEMS.2013.6713324.

[36]   A. Bogdanovs, O. Krievs, and J. Pforr, "Indirect Multiple DC Link Current Sensing Using Op-Amp Circuits in a Three-Phase Three-Level PWM Inverter," *PCIM Europe digital days 2021; International Exhibition and Conference for Power Electronics, Intelligent Motion, Renewable Energy and Energy Management*, Online, 2021, pp. 1–8.

[37]   A. Bogdanovs, O. Krievs, L. Ribickis, and J. Pforr, "Fuzzy Logic Current Balancing Controller Implementation in an Automotive Multi-Phase DC Converter with Coupled Inductors," *2020 IEEE 61th International Scientific Conference on Power and Electrical Engineering of Riga Technical University (RTUCON)*, Riga, Latvia, 2020, pp. 1–10, doi: 10.1109/RTUCON51174.2020.9316473.

[38]   O. Krievs and L. Ribickis, "Application of Fuzzy Logic Controllers in Industrial Electronics and Electrical Drives," *Power and Electrical Engineering*, vol. 5, 2002, pp. 77–85, ISSN 1407-7345.

[39]   L. J. Álvarez et al., "Design, analysis and modeling of an optimized fuzzy control algorithm for synchronous multiphase DC-DC converters in automotive applications," *2006 37th IEEE Power Electronics Specialists Conference*, Jeju, Korea (South), 2006, pp. 1–6, doi: 10.1109/pesc.2006.1712047.

[40]   C. Dhanalakshmi, A. Saravanan, and R. Jeba Raj, "Current Balancing in Multiphase Converter Based on Interleaving Technique using Fuzzy Logic," *International Journal of Engineering Sciences & Research Technology*, vol. 4, 2015, pp. 80–89.

[41]   X. Cui, W. Shen, Y. Zhang, and C. Hu, "A Fast Multi-Switched Inductor Balancing System Based on a Fuzzy Logic Controller for Lithium-Ion Battery Packs in Electric Vehicles," *Energies*, vol. 10, no. 7, p. 1034, Jul. 2017, doi: 10.3390/en10071034.

[42]   M. Murken and P. Gratzfeld, "Reliability Comparison of Bidirectional Automotive DC/DC Converters," *2017 IEEE 86th Vehicular Technology Conference (VTC-Fall)*, 2017, pp. 1–7, doi: 10.1109/VTCFall.2017.8288329.

[43] W. May and J. Pforr, "Design of integrated inductors in multi-phase buck/boost converters including operation with deactivated phases," *PCIM Europe 2019; International Exhibition and Conference for Power Electronics, Intelligent Motion, Renewable Energy and Energy Management*, Nuremberg, Germany, 2019, pp. 1–8.

[44] S. Utz and J. Pforr, "Operation of multi-phase converters with coupled inductors at reduced numbers of phases," *Proceedings of the 2011 14th European Conference on Power Electronics and Applications*, Birmingham, UK, 2011, pp. 1–10.

[45] A. Bogdanovs, O. Krievs, and J. Pforr, "Fault Detection using Indirect DC Link Current Measurement Technique in Multiphase DC Converter with Coupled Inductor," *2021 23rd European Conference on Power Electronics and Applications (EPE'21 ECCE Europe)*, Ghent, Belgium, 2021, pp. P.1–P.10, doi: 10.23919/EPE21ECCEEurope50061.2021.9570190.

[46] A. Bogdanovs, O. Krievs, and J. Pforr, "Fault-Tolerant Operation Algorithm for a Multi-Phase DC Converter with Coupled Inductors," *PCIM Europe 2022; International Exhibition and Conference for Power Electronics, Intelligent Motion, Renewable Energy and Energy Management, Nuremberg*, Germany, 2022, pp. 1–10, doi: 10.30420/565822070.

[47] K. Ma, H. Wang, and F. Blaabjerg, "New Approaches to Reliability Assessment: Using physics-of-failure for prediction and design in power electronics systems." In: *IEEE Power Electronics Magazine*, vol. 3, no. 4, pp. 28–41, Dec. 2016, doi: 10.1109/MPEL.2016.2615277.

[48] H. Wang and F. Blaabjerg, "Power Electronics Reliability: State of the Art and Outlook." In: *IEEE Journal of Emerging and Selected Topics in Power Electronics*, vol. 9, no. 6, pp. 6476–6493, Dec. 2021, doi: 10.1109/JESTPE.2020.3037161.

[49] F. Blaabjerg, H. Wang, I. Vernica, B. Liu, and P. Davari, "Reliability of Power Electronic Systems for EV/HEV Applications." In: *Proceedings of the IEEE*, vol. 109, no. 6, pp. 1060–1076, June 2021, doi: 10.1109/JPROC.2020.3031041.

[50] J. Schuderer et al., "Health Management of Power Electronics Systems," *PCIM Europe digital days 2021; International Exhibition and Conference for Power Electronics, Intelligent Motion, Renewable Energy and Energy Management*, 2021, pp. 948–955

[51] M. Ashourloo et al., "An Automotive-Grade Monolithic Masterless Fault-Tolerant Hybrid Dickson DC–DC Converter for 48-V Multi-Phase Applications." In: *IEEE Journal of Solid-State Circuits*, vol. 56, no. 12, pp. 3608–3618, Dec. 2021, doi: 10.1109/JSSC.2021.3105358.

[52] G. Selvaraj, A. R. Sadat, H. S. Krishnamoorthy, and K. Rajashekara, "An Improved Fault-Tolerant Power Converter for Electric Vehicle Propulsion," *2020 IEEE International Conference on Power Electronics, Smart Grid and Renewable Energy (PESGRE2020)*, 2020, pp. 1–5, doi: 10.1109/PESGRE45664.2020.9070596.

[53] S. Siouane, S. Jovanović, and P. Poure, "Open-Switch Fault-Tolerant Operation of a Two-Stage Buck/Buck–Boost Converter with Redundant Synchronous Switch for PV Systems." In: *IEEE Transactions on Industrial Electronics*, vol. 66, no. 5, pp. 3938–3947, May 2019, doi: 10.1109/TIE.2018.2847653.

[54] S. Kumar and B. S. Rajpurohit, "A Novel Fault Tolerant Control Scheme for Power Converter," *2020 IEEE International Power and Renewable Energy Conference*, 2020, pp. 1–5, doi: 10.1109/IPRECON49514.2020.9315247.

[55] E. Pazouki, J. A. De Abreu-Garcia, and Y. Sozer, "A Novel Fault-Tolerant Control Method for Interleaved DC–DC Converters Under Switch Fault Condition." In: *IEEE Transactions on Industry Applications*, vol. 56, no. 1, pp. 519–526, Jan.–Feb. 2020, doi: 10.1109/TIA.2019.2953030.

[56] M. M. Hillesheim, M. Cousineau, and L. Hureau, "Reconfigurable Partial-Decentralized Control of a Multiphase Converter for Fail-Operational Automotive Processor Power Supply," *2019 21st European Conference on Power Electronics and Applications (EPE '19 ECCE Europe)*, 2019, pp. P.1–P.8, doi: 10.23919/EPE.2019.8915561.

[57] M. Gleissner and M. Bakran, "Influence of inverse coupled inductors on fault-tolerant operation of two-phase DC-DC converters," *2015 17th European Conference on Power Electronics and Applications (EPE'15 ECCE-Europe)*, 2015, pp. 1–11, doi: 10.1109/EPE.2015.7309059.

[58] S. Utz, M. Stadler, and J. Pforr, "ACTIVE phase-shift control of multi-phase converters to minimize input current sub-harmonics," *2009 13th European Conference on Power Electronics and Applications*, Barcelona, Spain, 2009, pp. 1–10.

[59] G. Iannaccone, C. Sbrana, I. Morelli, and S. Strangio, "Power Electronics Based on Wide-Bandgap Semiconductors: Opportunities and Challenges." In: *IEEE Access*, vol. 9, pp. 139446–139456, 2021, doi: 10.1109/ACCESS.2021.3118897.

[60] J. W. Kolar and J. Huber, "Next-Generation SiC/GaN Three-Phase Variable-Speed Drive Inverter Concepts," *PCIM Europe digital days 2021; International Exhibition and Conference for Power Electronics, Intelligent Motion, Renewable Energy and Energy Management*, 2021, pp. 1–5.

[61] J. W. Kolar et al., "Application of WBG Power Devices in Future 3-Φ Variable Speed Drive Inverter Systems "How to Handle a Double-Edged Sword," *2020 IEEE International Electron Devices Meeting (IEDM)*, 2020, pp. 27.7.1–27.7.4, doi: 10.1109/IEDM13553.2020.9372022.

[62] E. Shelton et al., "Fast Switching of High Current WBG Power Devices," *PCIM Europe 2022*, 2022, pp. 1–8, doi: 10.30420/565822136.

[63] E. Gurpinar and A. Castellazzi, "Single-Phase T-Type Inverter Performance Benchmark Using Si IGBTs, SiC MOSFETs, and GaN HEMTs." In: *IEEE Transactions on Power Electronics*, vol. 31, no. 10, pp. 7148–7160, Oct. 2016, doi: 10.1109/TPEL.2015.2506400.

[64] H. Liu, T. Zhao and X. Wu, "Performance Evaluation of Si/SiC Hybrid Switch-Based Three-Level Active Neutral-Point-Clamped Inverter." In: *IEEE Open Journal of Industry Applications*, vol. 3, pp. 90–103, 2022, doi: 10.1109/OJIA.2022.3179225.

[65] M. J. Kasper, J. A. Anderson, G. Deboy, Y. Li, M. Haider, and J. W. Kolar, "Next Generation GaN-based Architectures: From 240W USB-C Adapters to 11kW EV On-Board Chargers with Ultra-high Power Density and Wide Output Voltage Range,"

PCIM Europe 2022; International Exhibition and Conference for Power Electronics, Intelligent Motion, Renewable Energy and Energy Management, 2022, pp. 1–10, doi: 10.30420/565822004.

[66] J. Azurza Anderson, G. Zulauf, J. W. Kolar, and G. Deboy, "New Figure-of-Merit Combining Semiconductor and Multi-Level Converter Properties." In: *IEEE Open Journal of Power Electronics*, vol. 1, pp. 322–338, 2020, doi: 10.1109/OJPEL.2020.3018220.

[67] K. Kroics, "WBG semiconductors, interleaving and integration of magnetics for non-isolated DC-DC converter performance improvement," *2020 XI National Conference with International Participation (ELECTRONICA)*, Sofia, Bulgaria, 2020, pp. 1–7, doi: 10.1109/ELECTRONICA50406.2020.9305134.

[68] Mustafeez-ul-Hassan, A. I. Emon, F. Luo, and V. Solovyov, "Design and Validation of a 20 kVA, Fully Cryogenic, 2-Level GaN Based Current Source Inverter for Full Electric Aircrafts." In: *IEEE Transactions on Transportation Electrification*, doi: 10.1109/TTE.2022.3176842.

[69] I. -S. Lee, J. -Y. Kang, J. Lee, and S. -T. Lee, "Design Considerations of Auxiliary Power Supply Unit with SiC MOSFET for Lightweight Railway Vehicles," *2018 21st International Conference on Electrical Machines and Systems (ICEMS)*, 2018, pp. 908–915, doi: 10.23919/ICEMS.2018.8549234.

[70] D. Wu, C. Xiao, H. Zhang, and W. Liang, "Development of auxiliary converter based on 1700V/325A full SiC MOSFET for urban rail transit vehicles," *2017 IEEE Transportation Electrification Conference and Expo, Asia-Pacific (ITEC Asia-Pacific)*, 2017, pp. 1–6, doi: 10.1109/ITEC-AP.2017.8080769.

[71] M. -A. Ocklenburg, M. Döhmen, X. -Q. Wu, and M. Helsper, "Next generation DC-DC converters for Auxiliary Power Supplies with SiC MOSFETs," *2018 IEEE International Conference on Electrical Systems for Aircraft, Railway, Ship Propulsion and Road Vehicles & International Transportation Electrification Conference (ESARS-ITEC)*, 2018, pp. 1–6, doi: 10.1109/ESARS-ITEC.2018.8607463

[72] I. Evtimov, R. Ivanov, and M. Sapundjiev, "Energy consumption of auxiliary systems of electric cars," in *MATEC Web Conf.*, 2017, vol. 133, pp. 1–5.

[73] Z. Biel, M. Šuňal, and P. Kulha, "Application of inverter parallel operation strategy in railway auxiliary converters," *2022 International Conference on Applied Electronics (AE)*, Pilsen, Czech Republic, 2022, pp. 1–4.

[74] A. Sheir, M. Z. Youssef, and M. Orabi, "A Novel Auxiliary Modular Inverter with Battery Integration for Electric Vehicle Applications," *2019 IEEE Applied Power Electronics Conference and Exposition (APEC)*, Anaheim, CA, USA, 2019, pp. 1730–1737, doi: 10.1109/APEC.2019.8721803.

[75] O. Sliskis, I. Dvornikovs, M. Marinbahs, J. Marks, and E. Groza, "Investigation of electrical bus traction motor dynamic using methods of physical and computer simulation," *2019 16th Conference on Electrical Machines, Drives and Power Systems (ELMA)*, Varna, Bulgaria, 2019, pp. 1–4, doi: 10.1109/ELMA.2019.8771668.

Artūrs Bogdanovs was born in 1989 in Riga. He received a Bachelor's degree in Automotive Engineering from Riga Technical University (Latvia) in 2014 and a Master's degree in Automotive Engineering from the University of Applied Sciences Ingolstadt (Germany) in 2017. He has worked as a power electronics engineer at Riga Electric Machine Building Factory. Since 2020 he has worked at Riga Technical University, where he currently is a researcher and a lecturer. His research interests include DC converters, auxiliary power supplies, automotive power electronics, control engineering, e-mobility, and engineering education.